THESIS

MODELING WIND IN COMPLEX TERRAIN FOR USE IN FIRE SPREAD PREDICTION

Submitted by

Jason M. Forthofer

Department of Forest, Rangeland, and Watershed Stewardship

In partial fulfillment of the requirements

For the Degree of Master of Science

Colorado State University

Fort Collins, Colorado

Summer 2007

COLORADO STATE UNIVERSITY

May 11, 2007

WE HEREBY RECOMMEND THAT THE THESIS PREPARED UNDER OUR SUPERVISION BY JASON FORTHOFER ENTITLED MODELING WIND IN COMPLEX TERRAIN FOR USE IN FIRE SPREAD PREDICTION BE ACCEPTED AS FULLFILLING IN PART REQUIREMENTS FOR THE DEGREE OF MASTER OF SCIENCE.

Committee on Graduate Work

(Please print name under signature)

_____

_____

_____

_____

_____

_____

_____

_____

Adviser

_____

_____

Department Head

ABSTRACT OF THESIS

MODELING WIND IN COMPLEX TERRAIN FOR USE IN FIRE SPREAD PREDICTION

Currently, no methods of predicting microscale, terrain influenced winds are available to fire managers. This study evaluated three methods of providing surface wind information to fire growth models. One was simply a uniform wind speed and direction, a method that has been traditionally used, and the other two types were based on numerical models used in the pollutant dispersion and wind power generation fields. The models were a commercial computational fluid dynamics (CFD) model and a mass-consistent model.

The accuracy of the models in simulating flow fields over two terrains with available measured data was assessed. While both models performed well on the upwind and tops of hills, the mass-consistent model had significant error on the lee side. The CFD model did better here.

The effect of the simulated flow fields on fire spread was examined using the FARSITE model. Comparison of using the simulated wind fields and traditional uniform wind fields was highlighted. Two historical fires with available weather and

fire progression were simulated. An important finding was that both wind models produced more accurate fire spread than the uniform winds. The CFD results were the most accurate, followed by the mass-consistent and then the uniform wind fields. Another important finding was that fire spread was less sensitive to input wind direction with the simulated winds than with the uniform winds. This could benefit fire modelers trying to predict fire spread when wind direction is not known accurately.

The study showed that both the CFD and mass-consistent wind model would be a useful addition to current fire behavior prediction systems. The CFD model appears to be more accurate, but the mass-consistent model has much shorter run times which could be an advantage, given short time constraints or limited computing resources.

Jason Michael Forthofer
Department of Forest, Rangeland, and Watershed Stewardship
Colorado State University
Fort Collins, CO 80523
Summer 2007

ACKNOWLEDGEMENTS

The author would like to thank the following people:

Dr. Bret Butler, for his expert supervision and encouragement throughout this process. Also, for obtaining the funding that made this thesis possible.

Professor Phil Omi, Professor Bogusz Bienkiewicz, Dr. Bill Doe, and Dr. Bob Shaw, for their supervision and support.

Dr. Mark Finney, for programming hints, tips, and solutions and also for discussions about wildland fire behavior modeling.

Chuck McHugh and Rick Stratton, for insight and strategy related to wildland fire behavior modeling as well as GIS support.

Professor Eric Thompson, for help in understanding the finite element method.

Larry Bradshaw, for providing the experimental data for Waterworks Hill.

Dr. Peter Taylor and Wensong Weng, for the Askerein Hill data set.

Kyle Shannon and Isaac Grenfell, for programming help and for a shoulder to cry on when things don't go as planned.

Funding for this thesis was provided by the Forest Service, U.S. Department of Agriculture, the Center for Environmental Management of Military Lands at Colorado State University, and the Joint Fire Science Program.

Finally, thanks to my parents for being such good role models and to my wife, Kelly, for her constant love and support.

CONTENTS

CHAPTER 1. INTRODUCTION

Wind is one of the most influential environmental factors affecting wildland fire behavior (Catchpole *et al.* 1998; Rothermel 1972). The mountainous terrain typical of many wildland fires produces complicated local wind patterns that make fire behavior prediction difficult. Indeed, the mechanical channeling and speed-up/speed-down effect of rough terrain on wind can be significant. Currently, fire managers rely on broad scale weather forecasts that do not describe localized terrain effects on wind. No method to compute winds in complex terrain is available to them.

Until recently, only Lopes (2002; 2003) had described a modeling system for predicting winds in complex terrain in a wildland fire context. His system did not catch on with the fire community, possibly because of deficiencies in the fire model used or a lack of much testing of both the fire and wind models. Preliminary work done for this study (Butler *et al.* 2006; Butler *et al.* 2004; Forthofer *et al.* 2003) has shown that models for predicting microscale winds for wildland fires are available and have the potential to provide useful information to fire managers. Most of these microscale wind models have been developed for the pollution dispersion and wind power generation fields.

The goals and objectives of this research are:

- to evaluate and/or develop methods for predicting microscale winds in complex terrain for wildland fire management purposes, and critically judge their performance in comparison with field data;
- to assess the use of microscale wind models in a spatially explicit fire behavior model, utilizing past fires and experimental wind databases for comparison;
- to provide guidance to the fire management community on the use of microscale wind models

The organization and layout of this thesis has been done in such a way as to facilitate adaptation to journal manuscripts easily in the future. The three main chapters (Chapters 2, 3, and 4) are written to be self-contained.

Chapter 1 provides an introduction to the problem area and states the goals and objectives of the study. Chapter 2 describes the computational fluid dynamics (CFD) model. Comparisons of model simulations with measured wind data are made for flow over a low, isolated hill and over moderately complex terrain. In Chapter 3, a simpler mass-consistent wind flow model is described. The sensitivity of several of the input variables is examined and recommendations are given. Model simulations are compared to the same data as the CFD model comparisons. Chapter 4 deals with using the simulated wind fields in a fire spread model. The differences in using the two types of simulated wind fields and the traditional method of spatially uniform winds is highlighted. Accuracy assessment of the fire growth predictions using different wind fields is accomplished by comparison to documented fire spread. Chapter 5

summarizes the research findings and performance of the wind models. Recommendations for future studies are also discussed.

CHAPTER 2. COMPUTATIONAL FLUID DYNAMICS WIND MODEL

2.1 Introduction

Wildland fires burning in mountainous terrain are often affected by complex, spatially heterogeneous wind patterns. The changes in direction and speed caused by terrain's effect on local winds contribute to erratic, varied fire behavior that is difficult to predict. Accurate simulation of these winds has been shown to improve fire behavior prediction (Butler *et al.* 2006). In fact, fine scale winds may be necessary to predict even the larger scale features of a fire's progression. Until recently, such a wind model has not been available to fire managers.

The global circulation and mesoscale models used by weather forecasters are not suitable for simulating winds at the scale necessary for fire behavior prediction. First, the hydrostatic approximation used in many models assumes that there is a balance between gravity and the pressure field. But at the small scales needed to simulate local wind effects, the pressure changes due to inertial effects in the vertical direction cannot be neglected. Also, the mesoscale models cannot resolve the variations in topography in the vertical direction that are important to prediction of

local wind patterns which typically involve flow separations and recirculation eddies (Atkinson 1995; Kim *et al.* 2000).

Methods for simulating small scale atmospheric flows over topography have been developed for the wind energy and pollutant dispersion fields. The models are usually based on linearised equations, potential-flow solutions, or computational fluid dynamics (CFD). The latter has been shown to perform better than the others in steep terrain where recirculation zones occur (Lopes 2003). In these areas of separated flow, non-linear effects become important and the CFD models appear to be more appropriate (Stangroom 2004). Several authors have reported successful CFD models for simulation of the neutral stable atmospheric boundary layer in topography (Alm and Nygaard 1995; Apsley and Castro 1997; Castro *et al.* 2003; Kim *et al.* 2000; Lopes 2003; Maurizi *et al.* 1998; Raithby and Stubley 1987; Undheim *et al.* 2006). In these models, a k-epsilon turbulence closure was used. This type of turbulence model is the standard for general CFD use. Since the development of the original k-epsilon turbulence model (Jones and Launder 1972), several variants have evolved. Kim and Patel (2000) tested several of these models for performance in atmospheric boundary layer flow over hills with separation and recirculation. They found that the RNG $k-\varepsilon$ turbulence (Yakhot and Orszag 1986) model performed best.

The most popular spatial fire spread modeling system in operational use today is FARSITE (Finney 1998). It uses a one dimensional spread model (Rothermel 1972) that requires surface wind speeds. These winds are those that would occur if the fire was not burning and subsequently affecting the flow. This is a consequence of the

empirical nature of the one dimensional spread model. The wind speed parameter used in the model was measured prior to ignition of each wind tunnel test fire used for empirical correlation. So the wind parameter used in the model is the ambient wind unaffected by the fire. This approach to fire modeling allows simulation of the wind to be decoupled from the fire behavior. In the past, analysts running FARSITE have had to use spatially constant descriptions of wind because no model was available to better describe the wind.

The current work describes a numerical model aimed at simulating steady, spatially explicit winds in complex terrain at a scale applicable for use in fire behavior prediction. Simulations from the model are compared to full scale measured data for two different terrains. These terrains are Askervein Hill (Taylor and Teunissen 1983; Taylor and Teunissen 1985) and Waterworks Hill (Bradshaw 2004).

2.2 Wind Model

2.2.1 Equations of motion

The commercial CFD code Fluent® is used to simulate the neutral atmospheric boundary layer flow over terrain. Since this code is a general purpose fluid dynamics model, a detailed description of the sub models and settings used is necessary. More information about the code can be found in the Fluent® User's Guide (Fluent 2007).

The fluid is considered viscous, incompressible, and turbulent. The fluid density is constant and so there is no buoyancy term in the vertical momentum equation. The energy equation is therefore, not solved. The Coriolis force is neglected

because at the scales simulated its effect is small. Also, the geometry effects of the terrain are assumed to dominate over Coriolis effects. The governing mass and momentum equations for this type of flow are

$$\frac{\partial u_i}{\partial x_i} = 0 \tag{1}$$

$$\frac{\partial}{\partial x_j}\left(\rho u_i u_j\right) = -\frac{\partial p}{\partial x_i} + \frac{\partial}{\partial x_j}\left[\mu\left(\frac{\partial u_i}{\partial x_j} + \frac{\partial u_j}{\partial x_i}\right)\right] + \frac{\partial}{\partial x_j}\left(-\rho\overline{u_i' u_j'}\right) \tag{2}$$

where u_i is time averaged velocity, u_i' velocity perturbation, x_i Cartesian direction, p pressure, ρ density, and μ laminar viscosity. The momentum equation is the result of applying the Reynolds Averaging procedure to the Navier-Stokes equations. The Reynolds stresses, $-\rho\overline{u_i' u_j'}$, are modeled using the Boussinesq hypothesis (Boussinesq 1877):

$$-\rho\overline{u_i' u_j'} = \mu_t\left(\frac{\partial u_i}{\partial x_j} + \frac{\partial u_j}{\partial x_i}\right) - \frac{2}{3}k\delta_{ij}\rho \tag{3}$$

where δ_{ij} is the Kronecker delta function. The turbulent viscosity, μ_t, is modeled using the RNG $k-\varepsilon$ turbulence model:

$$\mu_t = \rho C_\mu \frac{k^2}{\varepsilon} \tag{4}$$

where the turbulent kinetic energy, k, and the turbulence dissipation rate, ε, are modeled with transport equations:

$$\frac{\partial}{\partial x_i}\left(\rho k u_i\right) = \frac{\partial}{\partial x_j}\left(\frac{\mu_{eff}}{\sigma_k}\frac{\partial k}{\partial x_j}\right) + G_k - \rho\varepsilon \tag{5}$$

$$\frac{\partial}{\partial x_i}\left(\rho \varepsilon u_i\right) = \frac{\partial}{\partial x_j}\left(\frac{\mu_{eff}}{\sigma_\varepsilon}\frac{\partial \varepsilon}{\partial x_j}\right) + C_{1\varepsilon}\frac{\varepsilon}{k}G_k - C_{2\varepsilon}\rho\frac{\varepsilon^2}{k} - R_\varepsilon \tag{6}$$

The effective viscosity, μ_{eff}, is the sum of the laminar and turbulent viscosity. The quantities σ_k and σ_ε are the effective Prandtl numbers for k and ε. The production of turbulent kinetic energy, G_k, is computed as

$$G_k = 2\mu_{eff} S_{ij} S_{ij} \tag{7}$$

where S_{ij} is the mean strain-rate tensor:

$$S_{ij} = \frac{1}{2}\left(\frac{\partial u_i}{\partial x_j} + \frac{\partial u_j}{\partial x_i}\right) \tag{8}$$

The R_ε term in (6) is computed as

$$R_\varepsilon = \frac{C_\mu \rho \eta^3 \left(1 - \frac{\eta}{\eta_0}\right)}{1 + \beta\eta^3}\frac{\varepsilon^2}{k} \tag{9}$$

with $\eta = \sqrt{2S_{ij}S_{ij}}\,\frac{k}{\varepsilon}$, $\eta_0 = 4.38$, and $\beta = 0.012$. Other constants used are

$$C_\mu = 0.0845 \quad \sigma_k = 0.7179 \quad \sigma_\varepsilon = 0.7179$$

$$C_{1\varepsilon} = 1.42 \quad C_{2\varepsilon} = 1.68$$

This wind model assumes the atmosphere is neutrally stable. In reality, an absolutely neutral atmosphere is rare. Near neutral conditions are more common. So

the assumption of a neutrally stable atmosphere in the model becomes an approximation to the real atmosphere. Under high wind speeds typical of quickly spreading fires, there is sufficient mixing in the boundary layer that thermal effects can often be ignored (Byram and Nelson 1974; Parkinson 1987; Stangroom 2004).

The governing partial differential equations are discretized to produce a set of coupled, linear equations that can be solved. Second order central differencing is used for all diffusion terms and a second order upwinding scheme is used for the convective terms. Pressure-velocity coupling is achieved using the SIMPLEC (Vandoormaal and Raithby 1984) alogorithm. The equations are solved in a segregated way, using a point implicit solver (Gauss-Seidel) in conjunction with an algebraic multigrid method. All simulations were run until the residuals stopped decreasing.

2.2.2 Numerical Grids

The discretized equations are solved on unstructured, collocated numerical grids. This allows the use of more automatic meshing techniques and easier clustering of cells in certain domain areas than in structured grids. Other authors have also used unstructured grids for environmental flows with success (Kim and Boysan 1999; Stangroom 2004). For the simple terrain of Askervien Hill, an all hexahedral mesh has been used. A vertical stretching of the cells was used to concentrate cells near the ground where higher flow gradients occur. A hybrid mesh was used for the Waterworks Hill terrain because of the more complex, steep geometry. The mesh consisted of several layers of prismatic cells near the ground and tetrahedral cells

above. Both the prismatic cells and tetrahedral cells grow in size with increasing height.

2.2.3 Boundary Conditions

The boundary conditions at inlet surfaces are described by boundary layer profiles that are a function of height above the ground. The functional forms used are similar to those recommended by Richards and Hoxey (1993):

$$U = \frac{u_*}{K}\ln\left(\frac{z}{z_0}\right) \quad (10)$$

$$k = \frac{u_*^2}{\sqrt{C_\mu}} \quad (11)$$

$$\varepsilon = \frac{u_*^3}{Kz} \quad (12)$$

where U is horizontal velocity, K Von Karman's constant (0.41), z height above the ground, and z_0 is surface roughness length. The friction velocity, u_*, is computed as

$$u_* = \frac{KU_h}{\ln\left(\frac{h}{z_0}\right)} \quad (13)$$

where U_h is the wind velocity at some height above the ground h. These relations are incorporated using Fluent's® "user defined functions". Since the boundaries of the numerical grids used in this study may or may not line up with the dominant windspeed (i.e. the incoming wind direction is not parallel or perpendicular to any of the boundary

surfaces on the sides of the domain) there may be two inlet boundaries. These inlet boundaries have an incoming velocity magnitude equal to U in the appropriate oblique direction. Allowing wind directions not in line with the boundary surfaces permits using the same grid for multiple wind directions.

If the incoming wind direction happens to be aligned with the boundary surfaces, then the upstream surface will be an inlet surface and the two side surfaces are set to symmetry boundary conditions. Also, in all simulations the top boundary surface is set to a symmetry boundary condition. At these symmetry boundaries, the normal velocity component is set to zero and the normal gradients of all variables are set to zero. The boundary condition on outlet surfaces consists of setting the static pressure to a specified value and extrapolating all other values from the interior of the domain.

At the ground boundary, some discussion is necessary because the standard method used in Fluent® is not the same as is typically done in atmospheric boundary layer simulations. A no-slip condition is specified assuming the surface is aerodynamically rough by using a logarithmic relation to bridge the gap between the surface and the inertial sub-layer. For micro-scale atmospheric simulations, the following relation is normally used in the near wall cell.

$$U_p = \frac{u_*}{K} \ln\left(\frac{z_p}{z_0}\right) \qquad (14)$$

Here, U_p is the velocity at the cell center of the near wall cell and z_p is the distance from the ground to the cell center. In Fluent®, however, the following relation is used for fully rough walls.

$$\frac{U_p C_\mu^{\frac{1}{4}} k^{\frac{1}{2}}}{\frac{\tau_w}{\rho}} = \frac{1}{K} \ln\left(\frac{Ez_p \frac{\rho C_\mu^{\frac{1}{4}} k^{\frac{1}{2}}}{\mu}}{1 + C_s K_s \frac{\rho C_\mu^{\frac{1}{4}} k^{\frac{1}{2}}}{\mu}} \right) \quad (15)$$

Here τ_w is the wall shear stress, E is an empirical constant (=9.793), C_s is a roughness constant, and K_s is a roughness height. Since $u^* = \sqrt{\frac{\tau_w}{\rho}}$ and in an equilibrium turbulent boundary layer, $u^* = C_\mu^{\frac{1}{4}} k^{\frac{1}{2}}$, equation (15) can be rearranged to a form that resembles equation (14). To do this, an approximation must be made that the term $\frac{\mu}{\rho C_\mu^{\frac{1}{4}} k^{\frac{1}{2}}}$ is zero. The approximation is reasonable since for atmospheric flows, it is $O(10^{-5})$. The resulting equation is

$$U_p = \frac{u^*}{K} \ln\left(\frac{Ez_p}{C_s K_s} \right) \quad (16)$$

So, if $C_s = E$ and $K_s = z_0$, then equations (14) and (16) are equivalent and the usual atmospheric boundary layer wall condition has been implemented in Fluent®.

The boundary condition for k at the wall is that $\frac{\partial k}{\partial n} = 0$ if n is the direction normal to the wall. The production of turbulent kinetic energy at the wall adjacent cells is computed assuming local equilibrium. The production of k is computed as

$$G_k = \tau_w \frac{\tau_w}{K \rho C_\mu^{\frac{1}{4}} k_p^{\frac{1}{2}} z_p} \quad (17)$$

and ε is computed from

$$\varepsilon_p = \frac{C_\mu^{\frac{3}{4}} k_p^{\frac{3}{2}}}{Kz_p} \qquad (18)$$

Note that the ε transport equation is not solved in the near wall cells, but directly computed from equation (18).

In the current implementation of the wind model, the surface roughness length must be constant over the entire domain. It would be possible to allow roughness length to change over the terrain. However, this would require spatially explicit roughness information be available.

2.3 Simulation Results

Two sets of simulations for different terrains are presented. The simulation results are compared to full scale measurements.

2.3.1 Askervein Hill

Askervein Hill in Scotland was the site of an extensive wind data collection program in 1982 and 1983 (Taylor and Teunissen 1983; Taylor and Teunissen 1985). The program's goal was to compile data for neutral atmospheric flow over an isolated, low hill for use in validating wind energy models. Askervein Hill is 116 meters high, surrounded by relatively flat ground, and covered by low grass and heather. Over 50 towers were deployed and instrumented for wind measurements. The towers were placed approximately 100 meters apart along three lines running over the hill. Figure 1 shows 5 meter contour lines of elevation in the hill area and Lines A, AA, and B along

which the towers were deployed. The data used here are ten minute averaged winds from 10 meters above the ground. The elevation data used in this study are the 'Map B' data from Walmsley and Taylor (1996). These data provide a good opportunity to test the wind model.

The specific data sets used in the current study are called MF03-D and TU03B. These data correspond to a flow of 8.9 m/s from a direction of 210 degrees at 10 meters above the ground at a far upstream reference site. Atmospheric stability was near neutral (average Richardson numbers of -0.0110 to -0.0074). The roughness length used in the simulations was $z_0 = 0.03$ meters as suggested by Taylor and Teunissen (1983).

Two grids were built of differing resolution to assess the sensitivity of the solutions to the grids. The coarser grid consisted of approximately 500,000 cells. The first layer of cells above the ground was 1 meter tall and the average horizontal cell size was 40 meters. The fine grid had approximately 2,000,000 cells, 1 meter tall cells near the ground and an average horizontal cell size of 23 meters.

Figure 2, Figure 3, and Figure 4 compare the simulated results to those measured in the field campaign. As can be seen, there is considerable speed up of wind near the top of the hill. A sheltering effect is evident on the down wind side of the hill. The fine and coarse grid results are nearly identical, which suggests that both grids are of adequate resolution.

Both simulations produced results that were all within 2 m/s of the measured values. This corresponds to simulation points within 10 percent of the measured values

except at two measurement points. These two points are the right most two measurement points shown in Figure 2 and correspond to low wind speeds. Simulated values at these two points had errors of up to 32 percent. These larger errors on the lee side of the hill may be attributed to a time dependent recirculation zone that may have been present near the ground during the experiments (Castro *et al.* 2003). Other authors have suspected that hills downstream of Askervein not included in the simulations contributed to the poor prediction on the lee side of the hill (Kim and Patel 2000). It is also possible that inadequacies of the turbulence model arise in this area of nearly separated flow.

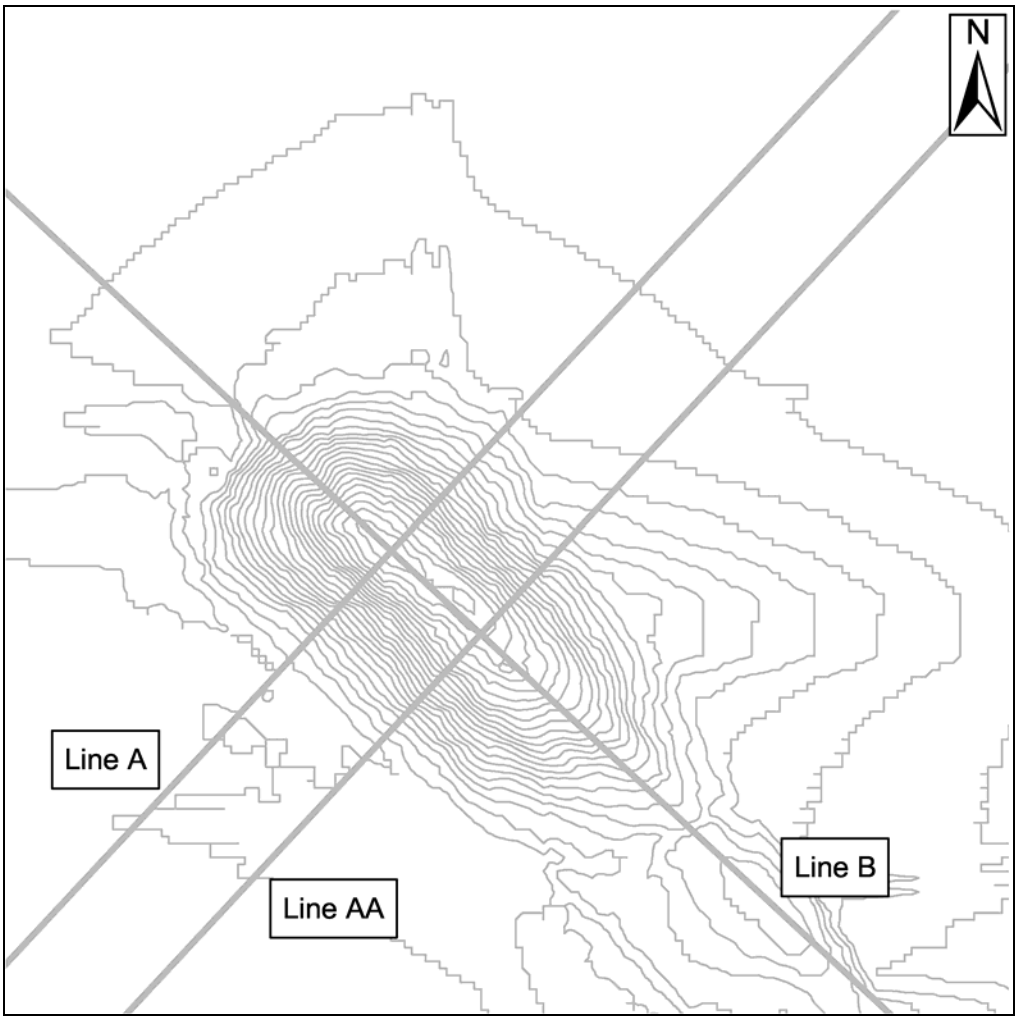

Figure 1. Contour map of Askervein Hill showing locations of Lines A, AA, and B. The contour interval is 5 meters.

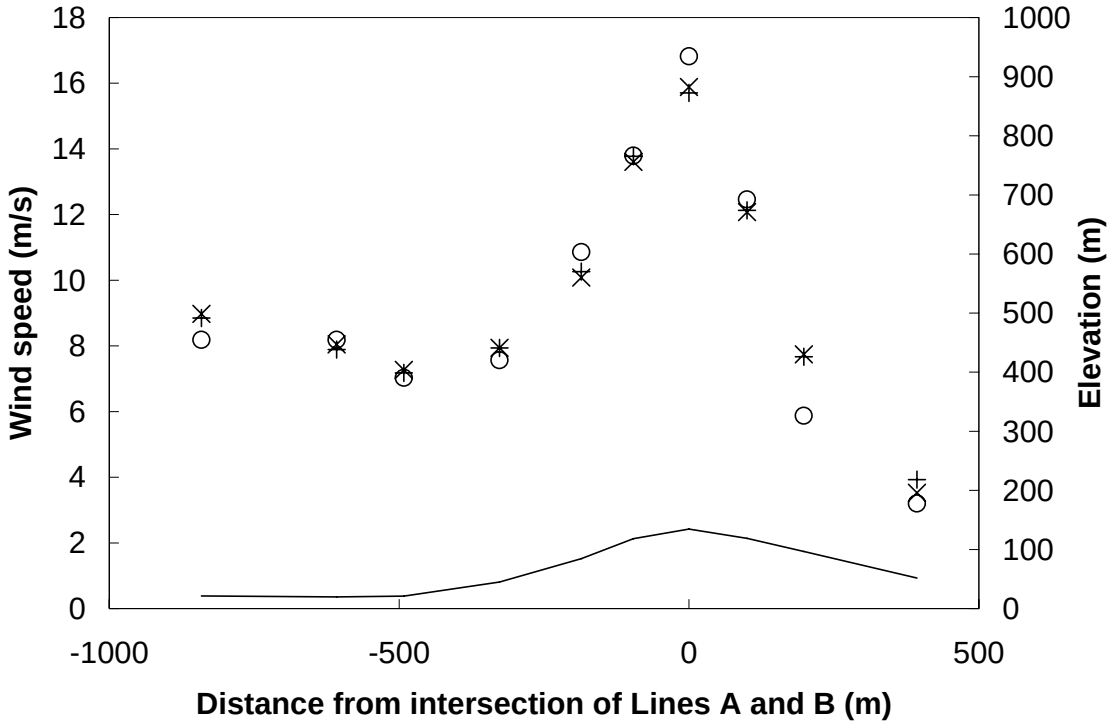

Figure 2. Wind speed along line A (Figure 1). Circles represent measured values, x's are the fine grid and plus symbols are the coarse grid. The solid line shows the elevation of Askervein hill.

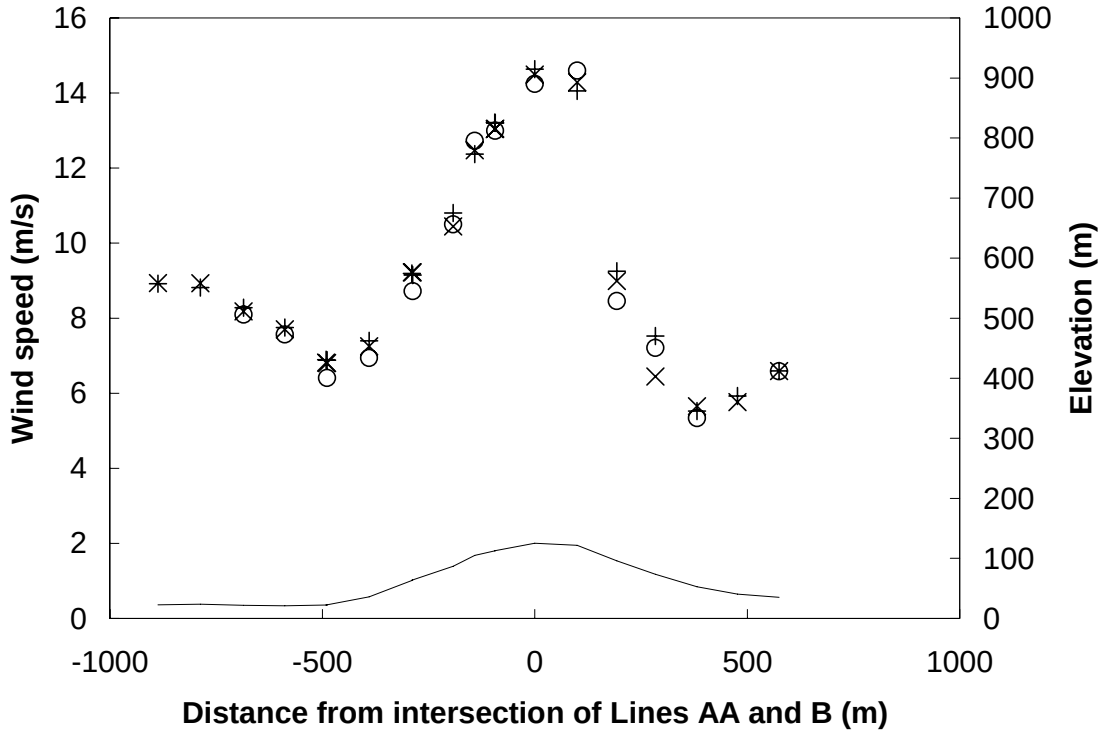

Figure 3. Wind speed along line AA (Figure 1). Circles represent measured values, x's are the fine grid and plus symbols are the coarse grid. The solid line shows the elevation of Askervein hill.

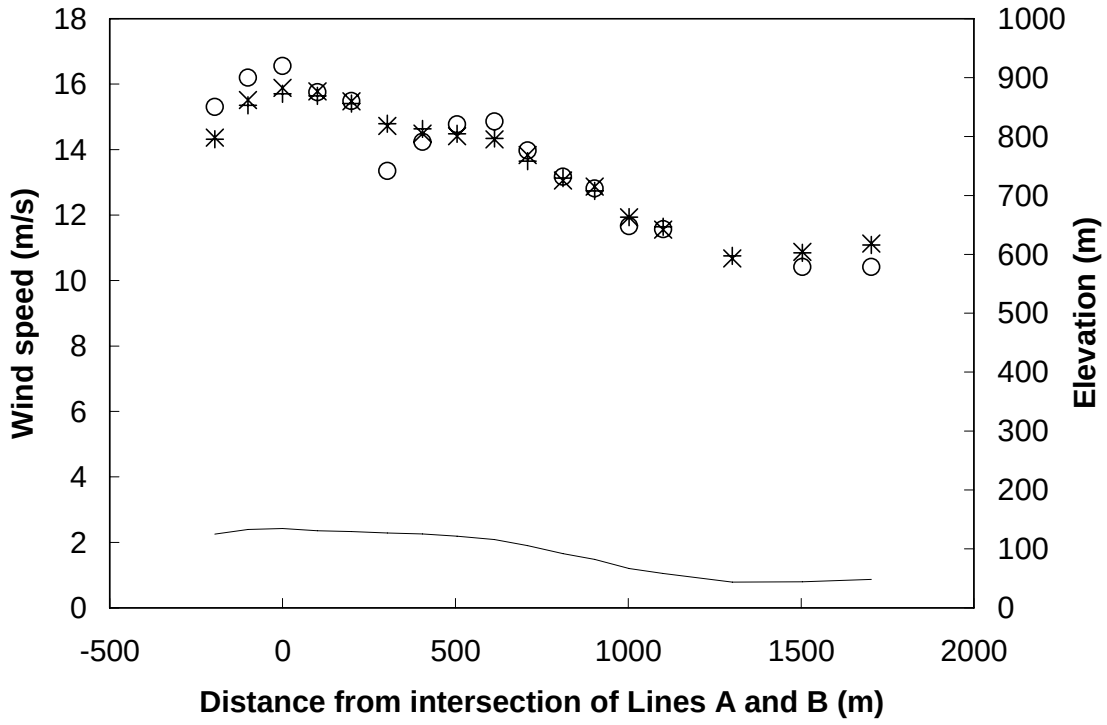

Figure 4. Wind speed along line B (Figure 1). Circles represent measured values, x's are the fine grid and plus symbols are the coarse grid. The solid line shows the elevation of Askervein hill.

2.3.2 Waterworks Hill

In July of 2004, the Missoula Fire Sciences Laboratory measured wind speeds over a hill near Missoula, MT named Waterworks Hill (Bradshaw 2004). The hill is approximately 200 meters tall and has a relatively flat upwind fetch to the West of over 10 kilometers. To the North, East, and South the hill is surrounded by larger hills and mountains. It is covered with grass that is approximately 8-30 centimeters tall.

Eleven wind measurement towers were placed on the hill and surrounding area, however, data from only 8 were available. The towers were 3.05 meters (10 feet) tall. Winds reported here are 30 minute averaged. A weather station operated by the National Weather Service located at the Missoula Airport was also used, making nine

total wind stations used here. This station is approximately 8 kilometers to the West-Northwest of the hill and measures winds at 10 meters above the ground. Winds were measured during a cold front passage that was characterized by strong winds for this area. For a period of 3 hours, averaged wind speeds at the Missoula Airport were consistently between 9.4 m/s and 10.3 m/s from the West. This station was used to set the incoming flow boundary condition for the simulations.

The elevation data used in the simulation were obtained from USGS (USGS 2006). The domain size was approximately 21 kilometers by 16 kilometers and is shown in Figure 5. The resolution of the elevation data was 30 meters. The top boundary of the computational domain was set at 5 kilometers above sea level.

Figure 5. Topography map of Waterworks Hill and surrounding area. North is toward the top of the image. The black triangles represent locations of wind measurement towers. The West most tower is the Missoula Airport tower and the East most tower is the Tulip tower. The other 10 towers are located on the actual hill. The elevation contour interval is 20 meters.

Two grids of differing resolution were used for the Waterworks Hill simulations to assess the sensitivity of the solutions to the grids. Each grid had eight layers of prismatic cells adjacent to the ground. The coarse grid consisted of a total of 842,000 cells. The height of the near wall cells was 12 meters, and the horizontal cell size near the ground was 80 meters. The fine grid had 1,529,000 cells, a near wall cell height of 5 meters, and a horizontal cell size near the ground of 62 meters.

Figure 6 and Figure 7 show vector plots of the simulated wind. Figure 8 graphically compares the results of the simulations to the measured data. Numerical values at each measurement station, including percent error, are listed in

Table 1. From these it is evident that the two meshes produced similar results. The fine mesh did, however, compare slightly better than the coarse mesh. This can be seen at stations FC1, FC3, FB1, and DV4. Since the change in wind speed is small from the fine mesh to the coarse mesh, these simulations appear to be relatively insensitive to the meshes used and a near mesh independent solution was obtained.

Both the coarse and fine simulations under-predicted the velocities at the higher elevation towers that had the strongest winds. The reasons for this are not clear; however, at least two possibilities are hypothesized. The first is that the atmosphere was not of neutral stability during the measurement period. It is possible that buoyancy effects produced higher wind speeds near the top of the hill. Another possible explanation for the under-prediction is that terrain features upwind of the Missoula Airport reference site may have disturbed the flow measured at this tower. The terrain is flat for approximately seven kilometers upwind of the tower, but further upwind a large mountain range exists. It is possible that this upwind mountain range sheltered the Missoula Airport reference site. This would mean that the logarithmic boundary layer profile used as input to the simulations was incorrect and that wind at the higher altitudes was stronger. Either of these possibilities could have acted separately or together to produce the under-predictions near the hill top.

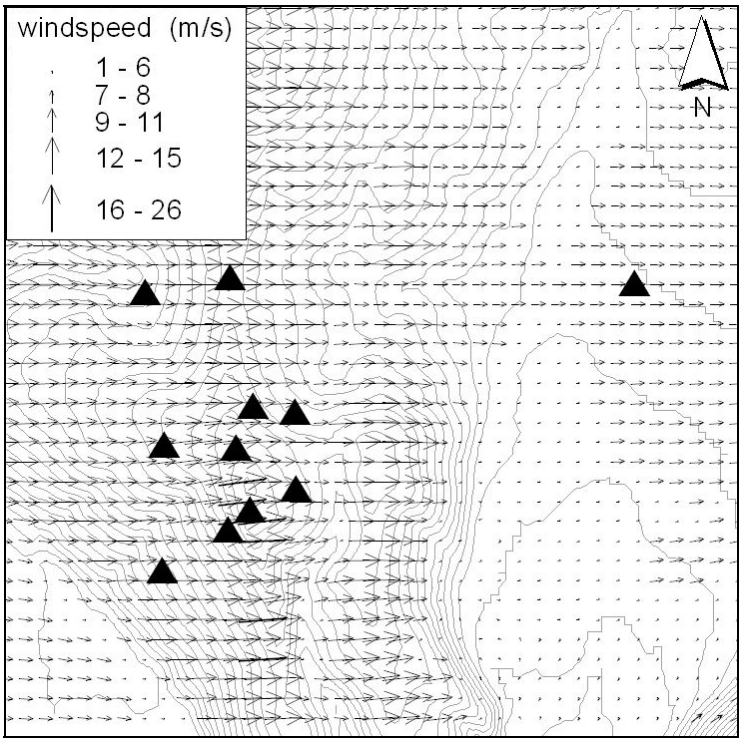

Figure 6. Wind vector plot of simulated flow using the coarse mesh in the Waterworks Hill area. The vectors are spaced on an 80 meter grid.

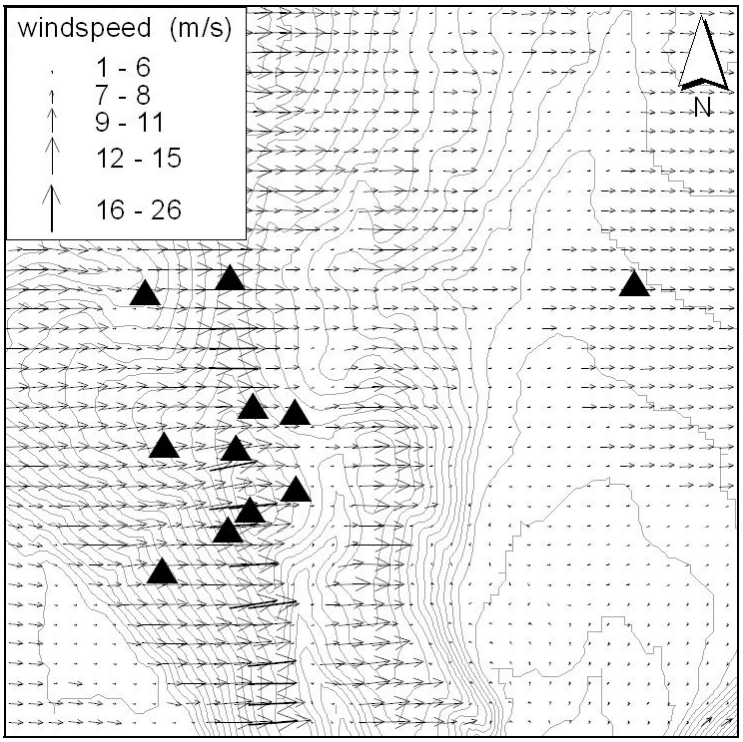

Figure 7. Wind vector plot of simulated flow using the fine mesh in the Waterworks Hill area. The vectors are spaced on an 80 meter grid.

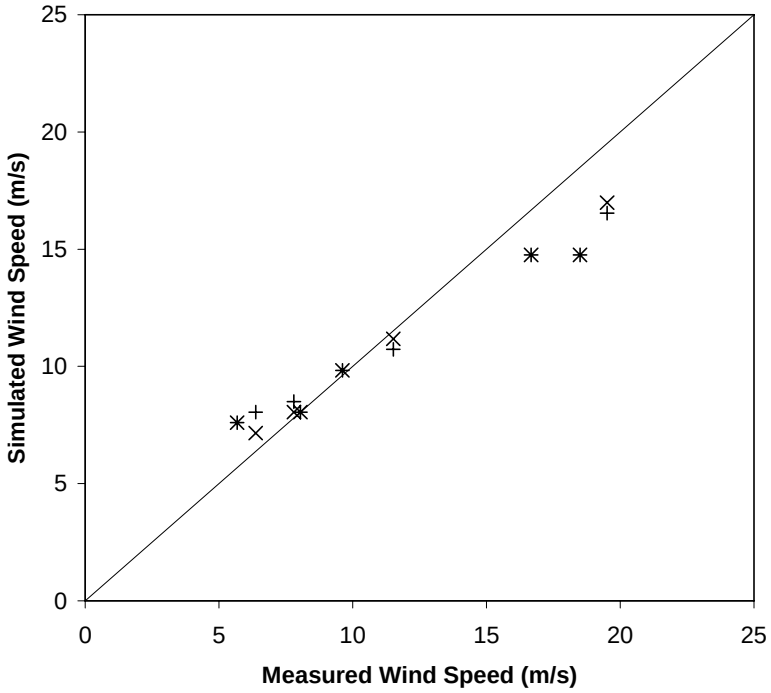

Figure 8. Comparison of simulated and observed wind speeds over Waterworks Hill. The x's represent the fine grid and the + signs represent the coarse grid. The solid black line is the line of perfect agreement.

Table 1. Velocity comparison for Waterworks Hill.

Station		FC1	FC2	FC3	FB1	FB2	DV2	DV4	MSO	Tulip
Measured	velocity (m/s)	11.5	16.7	19.5	7.8	18.5	9.6	6.4	8.0	5.7
Fine mesh	velocity (m/s)	11.2	14.8	17.0	8.0	14.8	9.8	7.2	8.0	7.6
	error (%)	-2.9	-11.5	-12.9	3.1	-20.3	2.3	12.1	0.0	33.9
Coarse mesh	velocity (m/s)	10.7	14.8	16.5	8.5	14.8	9.8	8.0	8.0	7.6
	error (%)	-6.8	-11.5	-15.2	8.8	-20.3	2.3	26.2	0.0	33.9

The largest percent error of 33.9 percent occurred at the Tulip station. This station was located in the small valley in the lee of the hill. The roughness features in this valley are larger than on the hill, yet were not accounted for in the simulations. The valley has tree and brush vegetation as well as scattered, residential buildings. This may be the reason for the over-prediction of wind speed at this site.

2.4 Conclusions

Overall, the simulations compared to the measured data with a relatively high degree of accuracy. All simulations were within 34 percent of the measured values and most were less than 15 percent. This amount of error in wind speed should be acceptable to fire analysts, considering the typical errors in other fire behavior parameters and the accuracy of other available methods of obtaining wind information. Based on the two cases studied, the assumptions of the model appear to be appropriate. The results of the simulations suggest that the model could be very useful for wildland fire behavior prediction. Further case studies in terrain of higher complexity would be useful in determining the model accuracy in these situations.

CHAPTER 3. MASS-CONSISTENT WIND MODEL

3.1 Introduction

The behavior of a wildland fire is strongly influenced by the wind speed and direction acting at the location, or locations where the fire is burning (Rothermel 1972). Accurate prediction of these local, or microscale, winds can improve the accuracy of fire behavior predictions. This is especially true for fires burning in mountainous terrain that can heavily impact local winds. These terrains produce complicated spatial and temporal wind patterns that make fire behavior prediction difficult. In the past, fire managers have had to rely on expert judgment or large scale weather service forecasts to estimate local winds. Expert judgment can be unreliable, and has probably contributed to several firefighter entrapments and fatalities (see, for example Rothermel (1993), Butler et al. (1998) and USDA Forest Service and USDI Bureau of Land Management (2002)). Weather forecasts generally capture broad, large scale trends well, but do not provide detailed information on local, terrain influenced winds. This information would be valuable to fire managers.

Several numerical models have been proposed for simulating microscale wind effects. Most of these were developed for wind turbine siting or pollutant dispersion prediction. These models are generally called diagnostic models because they are

steady in time. Time stepping, or prognostic, models also exist but are usually designed for large scale (mesoscale or larger) weather prediction. These models include equations for the physics relevant to weather prediction such as conservation of mass, momentum, energy, moisture and radiant transfer. A disadvantage of these models is that their coarse resolution does not allow them to accurately simulate small scale terrain effects (Atkinson 1995; Kim *et al.* 2000). Also, they are computationally expensive. This may preclude them from seeing widespread use in wildland fire applications. Another problem is that the prognostic weather models require initial and boundary conditions that may be difficult to obtain, especially for a "what-if" type fire scenario. Because of these drawbacks, diagnostic models are better suited for predicting local winds for wildland fire use.

The diagnostic models can be classified into three categories according to the amount of physics incorporated. In the simplest category, called mass-consistent models, the only physics explicitly incorporated is the conservation of mass (Chan and Sugiyama 1997; Davis *et al.* 1984; Geai 1987; Montero *et al.* 1998; Moussiopoulos and Flassak 1986; Ross *et al.* 1988; Sherman 1978). Most attempt to obtain a divergence free flow while minimizing the change from some initial wind field. Other effects such as momentum or density driven flows can partially be accounted for if this information is present in the initial wind field. The more sophisticated mass-consistent models incorporate empirical parameterizations of phenomena such as non-neutral stability, kinematic effects and diurnal forcing (Scire *et al.* 2000). The big advantage of mass consistent models is the low computational expense. Simulations generally take from a few seconds to a few minutes on today's desktop or laptop computers.

At the other end of the spectrum are the most complicated diagnostic models. Models in this category include, at a minimum, conservation of mass and momentum equations with some form of turbulence closure (Alm and Nygaard 1995; Apsley and Castro 1997; Castro *et al.* 2003; Kim *et al.* 2000; Lopes 2003; Maurizi *et al.* 1998; Raithby and Stubley 1987; Uchida and Ohya 1999; Undheim *et al.* 2006). They may also include conservation of energy (Montavon 1998). These models are often called computational fluid dynamics (CFD) models. They have been shown to handle non-linear flow effects such as recirculation better than mass-consistent models because a momentum equation is solved (Lopes 2003). The downside of these models is that they are computationally more expensive. Simulations take from a few minutes to a few hours on today's personal computers.

The last diagnostic group, which falls between the mass-consistent and CFD models, is the dynamic linearized models group. These models solve a linearized momentum equation (Jackson and Hunt 1975; Mason and King 1985; Mortensen *et al.* 1993; Walmsley *et al.* 1986). Computation times of these models are similar to the mass-consistent models. Because of the approximate momentum equation solved, non-linear momentum effects occurring in steep terrain are not handled well (Lopes 2003). Walmsley et al. (1990) and Barnard (1991) compared dynamic linearized models and mass-consistent models and found that each gave similar results. Finardi et al. (1993) found that both types of models produced reasonable results, but that the linearized models might give better results when only one surface wind observation is available.

The model described in this paper belongs to the mass-consistent group. This type of model is being investigated because it appears to have certain advantages that

align well with wildland fire application. Computational cost is the major issue. The mass-consistent and dynamic linear models compute wind fields in seconds to a few minutes compared with the CFD models which can take one to two hours. Since timelines are often tight during wildland fires, the mass-consistent and dynamic linearized models may be more useful and practical, especially since more than one simulation is usually needed. The trade-off may be loss of some accuracy, especially in the wake region of a terrain feature. Lopes (2003) investigated both a CFD model and a mass-consistent model for wildland fire application and found that on the lee side of the isolated hill simulated, that the CFD model more closely matched measurements. In his complex mountainous terrain simulations, however, the CFD results did not show any improvement over the mass-consistent model. This could be attributed to a poor description of the approach flow, or local terrain features or roughness not accurately described (Lopes 2003). Another reason the mass conserving models may work well for fire applications is that they can be used in conjunction with large scale prognostic weather models easily. Interpolation can be used to obtain an initial wind field for the mass-consistent model from the coarse grid weather model data. Such a combination would account for both the mesoscale meteorology and the local terrain effects (Petersen *et al.* 1997).

This study will describe a mass-consistent model for predicting wind in complex terrain for wildland fire management use. Simulations from the model will be compared to data from two full-scale field studies. The first field study represents relatively simple flow over a low, isolated hill. The sensitivity of the model will be tested against these data. The second field study represents more complex terrain.

Simulations of the model will be performed to assess the accuracy of the model and to give an example of the model being used in real terrain.

3.2 Numerical Model

3.2.1 Governing equations

The model seeks to minimize the change from an initial wind field while conserving mass. The variational calculus techniques used were developed by Sasaki (1958; 1970a; 1970b).

The function to minimize is constructed using the square of the difference between the adjusted and observed values, as shown below.

$$E(u,v,w) = \int_{\Omega} \left[\alpha_1^2 (u-u_0)^2 + \alpha_1^2 (v-v_0)^2 + \alpha_2^2 (w-w_0)^2 \right] d\Omega \qquad (19)$$

The computational domain is denoted by Ω, α_1 and α_2 are the Gauss precision moduli, u, v, and w are the velocity components in the x (positive to East), y (positive to North), and z (positive upward) directions, respectively. The initial values of velocity are u_0, v_0 and w_0. The minimum value of $E(u,v,w)$ will give the minimal change from the initial velocity field in a least squares sense. The Gauss precision moduli can be used to control the relative amount of change induced by the model to the horizontal and vertical directions. This is an attempt to account for some stability effects. A value of 1 for both moduli means that change in flow can occur equally in the horizontal and vertical directions. This would simulate a neutral stable atmosphere. An overview of methods for setting the Gauss precision moduli for non-neutral

conditions is found in Ratto et al. (1994). At this stage in the model, only neutral stability will be considered.

The minimization of (19) is subject to the strong constraint that the resulting wind field must conserve mass. The conservation of mass equation is

$$H(u_x, v_y, w_z) = \frac{\partial u}{\partial x} + \frac{\partial v}{\partial y} + \frac{\partial w}{\partial z} = 0 \qquad (20)$$

Using Lagrange multiplier theory, the problem becomes one of minimizing the modified functional $F(u, v, w, \lambda)$ shown below.

$$\begin{aligned} F(u, v, w, \lambda) &= E(u, v, w) + \int_\Omega \lambda H(u_x, v_y, w_z) d\Omega \qquad (21) \\ &= \int_\Omega \left[\alpha_1^2 (u - u_0)^2 + \alpha_1^2 (v - v_0)^2 + \alpha_2^2 (w - w_0)^2 + \lambda \left(\frac{\partial u}{\partial x} + \frac{\partial v}{\partial y} + \frac{\partial w}{\partial z} \right) \right] d\Omega \end{aligned}$$

Here, $\lambda(x, y, z)$ is a Lagrange multiplier. The minimum of (21) is found from the solution of the associated Euler-Lagrange equations.

$$\begin{aligned} & u = u_0 + \frac{1}{2\alpha_1^2} \frac{\partial \lambda}{\partial x}, \quad v = v_0 + \frac{1}{2\alpha_1^2} \frac{\partial \lambda}{\partial y}, \quad w = w_0 + \frac{1}{2\alpha_2^2} \frac{\partial \lambda}{\partial z} \qquad (22) \\ & \frac{\partial u}{\partial x} + \frac{\partial v}{\partial y} + \frac{\partial w}{\partial z} = 0 \end{aligned}$$

They are subject to the boundary condition that

$$\lambda \delta \vec{V} \cdot \vec{n} = 0 \quad on \quad \Gamma \qquad (23)$$

where Γ is the surface of the domain, $\vec{V} = (u, v, w)$, $\vec{n}$ is the outward unit vector normal to the surface of the domain, and $\delta \vec{V}$ is the first variation of the velocity.

The Euler-Lagrange equations (22) can be reduced to one equation by taking the partial derivatives of the first three equations (with respect to x, y, and z) and

substituting these into the last equation. To simplify notation, let $\alpha^2 = \alpha_1^2 / \alpha_2^2$ and $\alpha_1 = 1$. The result is an elliptic partial differential equation for λ, as shown below.

$$\frac{\partial^2 \lambda}{\partial x^2} + \frac{\partial^2 \lambda}{\partial y^2} + \alpha^2 \frac{\partial^2 \lambda}{\partial z^2} = -2\left(\frac{\partial u_0}{\partial x} + \frac{\partial v_0}{\partial y} + \frac{\partial w_0}{\partial z} \right) \qquad (24)$$

Once the $\lambda(x, y, z)$ field is found, the adjusted wind velocities can be computed from (22 **)**.

The boundary condition used on "open" or "flow-through" boundaries is $\lambda = 0$. This implies that the normal derivative is, in general, not zero which gives a non-zero adjustment to the normal velocity (see (22)). In the non-normal directions, the derivative is zero so no adjustment is made to those components of velocity. At the ground boundary, a Neumann condition is imposed, i.e. that $\frac{\partial \lambda}{\partial n} = 0$. This implies that the velocity normal to the ground surface is not adjusted from its initial value. Since the velocity at the ground nodes is initialized to zero, the adjusted velocity is also zero. This allows the ground boundary to act as an "impermeable" boundary.

3.2.2 Numerical Grid

The elliptic equation is solved on a simple, algebraically derived terrain following grid using Cartesian coordinates. A global terrain conformal coordinate system such as in Davis et al.(1984) and Ross et al.(1988) is not used. Instead, the finite element method used here performs a mapping from physical space to a computational space on an element by element basis. This allows the use of a terrain following grid rather than a stair stepped Cartesian grid, which has been shown to lead to large velocity errors near the surface (Lewellen *et al.* 1982). Also, the governing

equation does not need to be rewritten in the conformal coordinate system (introducing more terms) and then discretized. The grid used in this study consists of layers of hexahedral cells that grow in vertical size with height above the ground. This type of mesh gives higher resolution near the ground without penalizing efficiency.

3.2.3 Finite Element Solution Method

Numerical solution to (24) is obtained using usual finite element techniques, described in, for example, Thompson (2005). The elliptic Poisson's equation for λ is written in a weak form and Galerkin's method is used. The resulting finite element equation for an element is shown in (25) and (26). Eight node isoparametric hexahedral elements and the corresponding low-order shape functions are used for integration as well as interpolation. The resulting system of coupled, linear, algebraic equations are solved using a Conjugate Gradient method with Jacobi preconditioning (Barrett *et al.* 1994). To reduce memory requirements, a compressed row storage format was implemented for the stiffness matrix. Numerical integration is performed using Gaussian quadrature.

$$\left[\int_{\Omega_{uv}}\left[\left\{\frac{\partial N}{\partial x}\right\}\quad\left\{\frac{\partial N}{\partial y}\right\}\quad\left\{\frac{\partial N}{\partial z}\right\}\right]\begin{bmatrix}1&0&0\\0&1&0\\0&0&\alpha^2\end{bmatrix}\begin{bmatrix}\left[\frac{\partial N}{\partial x}\right]\\\left[\frac{\partial N}{\partial y}\right]\\\left[\frac{\partial N}{\partial z}\right]\end{bmatrix}\|J\|d\Omega\right]\{\lambda\} = \left[\int_{\Omega_{uv}}\{N\}H\|J\|d\Omega\right] \tag{25}$$

$$H = 2\left(\frac{\partial u_0}{\partial x} + \frac{\partial v_0}{\partial y} + \frac{\partial w_0}{\partial z}\right) = 2\left(\left[\frac{\partial N}{\partial x}\right]\{u_0\} + \left[\frac{\partial N}{\partial y}\right]\{v_0\} + \left[\frac{\partial N}{\partial z}\right]\{w_0\}\right) \quad (26)$$

3.2.4 Solution Initialization

The mass-consistent models are sensitive to the initial wind field (Chino and Ishikawa 1988). This is because the models minimize the change from this initial wind field. There are many possible ways to obtain the initial wind field needed by the numerical model. Often, the mass-consistent models initialize the domain using available measured data. Most models use some form of interpolation/extrapolation of measured data from surface weather stations and vertical profile measurements. Many incorporate theoretical vertical wind profiles because there are generally few or no measured vertical profiles. Stability effects can also be incorporated into these theoretical profiles. As discussed by Ratto et al. (1994), problems can be encountered using interpolation/extrapolation of measured surface data. If one or more of the measurement stations are located in areas that are strongly affected by localized phenomena, these data will adversely influence the initialized wind field. This occurs because the highly localized data influences a large area in the interpolation/extrapolation process. This could happen, for example, if a weather station were located in a lee side eddy, or if nearby vegetation or buildings affected the measurement. Because of these considerations, the authors of EOLOS (Lalas *et al.* 1988; Tombrou and Lalas 1990) and $\mathcal{WINDS}$ (Ratto *et al.* 1990) allow users the option to neglect the surface measurements and initialize the models using only the geostrophic wind.

Interpolation/extrapolation methods are, of course, only useful if measurement data are available. For wildland fire management use, there are many instances when virtually no data will be available. This may be because the area is very remote with few or no weather stations or the simulation is for a future time (a prediction). In these cases, only a guess about the geostrophic or gradient winds are available based on broad weather predictions or scenarios. For this reason, the current model does not include an interpolation/extrapolation methodology. Instead, the domain is initialized using a theoretical vertical wind profile based on a wind speed and direction at a standard height (usually 20 ft or 10 m). The wind profiles used are either standard logarithmic or power law functions with appropriate surface roughness parameterization.

In the future, interpolation/extrapolation schemes will be implemented. This will allow not only the option of using weather station data, but also use of coarse data from larger scale weather models such as MM5 (NCAR 2007), Weather Research and Forecasting (WRF) Model (Conrad 2007), or the National Digital Forecast Database (NDFD) (NWS Internet Services Team 2007).

3.3 Simulation Results

3.3.1 Askervein Hill

The most commonly used data set for validating local scale wind models for wind turbine siting is Askervein Hill (Taylor and Teunissen 1983; Taylor and Teunissen 1985). The hill is 116 meters high and surrounded by flat terrain covered by low grass and heather. It is located on the island of South Uist of Scotland. The wind collection program in 1982 and 1983 placed over 50 measurement towers on the hill.

Most of the towers were 10 meters tall and measurements reported here are 10 minute averages. There were also a few taller towers, up to 50 meters, and kite measurements taken at higher altitudes. The towers were spaced about 100 meters apart along three lines running over the hill. Figure 1 shows these lines, the topography of Askervein Hill, and the surrounding area. The Askervein data set will be used to evaluate the wind model.

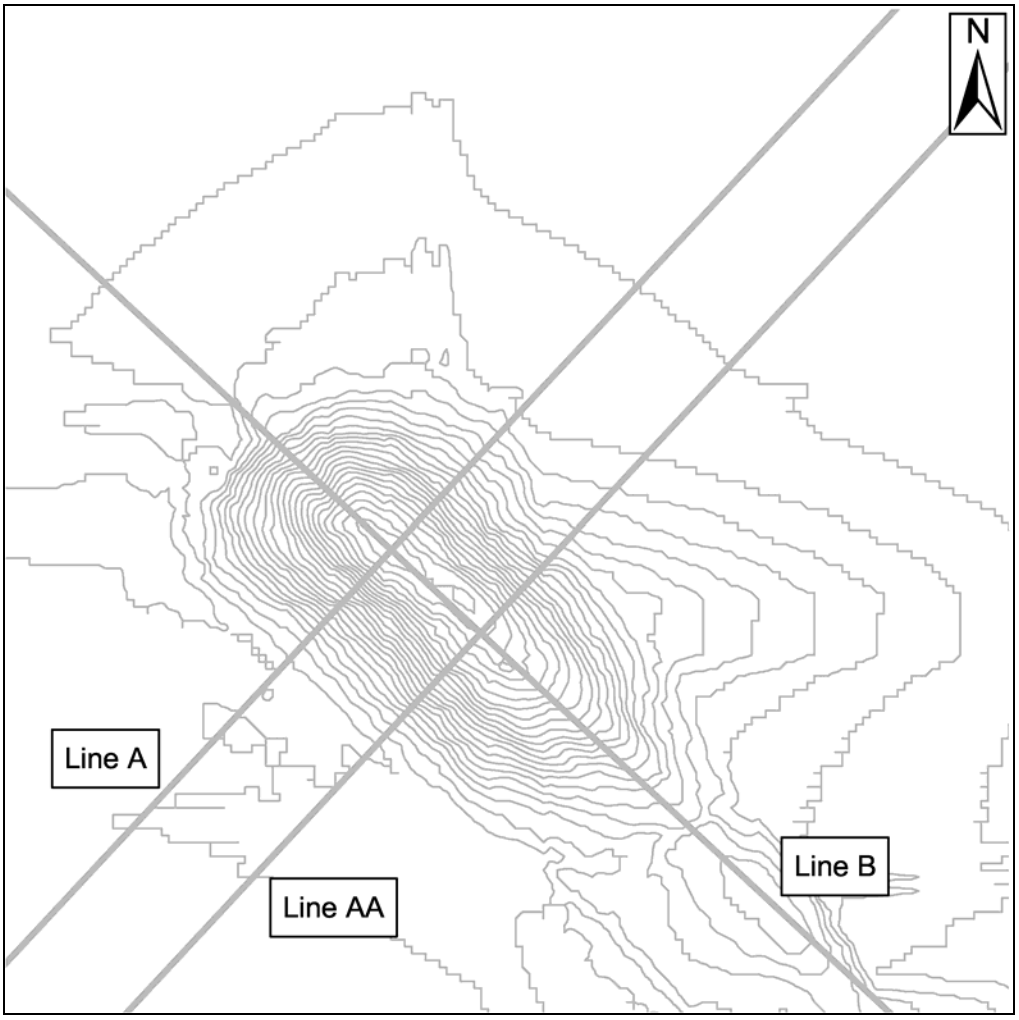

Figure 9. Contour map of Askervein Hill showing locations of Lines A, AA, and B. The contour interval is 5 meters.

The data sets used are MF03-D and TU03B from the 1983 field campaign (Taylor and Teunissen 1985). These data correspond to an average flow of 8.9 m/s

from a direction of 210 degrees at 10 meters above the ground at a far upstream reference site. The atmospheric stability was near neutral (average Richardson numbers of -0.0110 to -0.0074). The ground roughness length was $z_0 = 0.03$ meters as suggested in Taylor and Teunissen (1985). The digital elevation model used in the simulations is the 'Map B' elevation data described in Walmsley and Taylor (1996).

The Askervein Hill data set has a relatively dense spatial coverage of measurement towers compared to other field experiments. This makes the data an excellent candidate to use to examine the sensitivity of the numerical model to certain inputs. A base case was identified, and then several simulations were performed with varied input. All parameters other than the one under examination were held at the base case values unless noted. The parameters examined in the sensitivity study were: iteration residual tolerance, number of quadrature points used in the numerical integration, horizontal resolution, vertical resolution, and cell aspect ratio. They are discussed in detail in following sections. The parameters used in the base case are shown in Table 2.

Table 2. Base case parameters.

Residual tolerance	0.1
Number of quadrature points	1
Horizontal resolution	40 meters
Vertical resolution	20 cells, growth rate 30%
Cell aspect ratio	23

The mesh used in the simulations was rectangular and aligned with the cardinal directions. In both the North-South and East-West directions, the mesh had 6 kilometer sides. The hill was placed approximately in the center. The top of the

domain was 1000 meters above sea level. The area surrounding Askervein Hill is relatively flat and averages 8 meters above sea level.

The simulation domain was initialized using information from the vertical velocity profile data at the upstream reference site. A power law equation was fit to the data using the least squares technique and is shown in (27). Here, $V(z)$ is the velocity and z is the height above the ground. The entire simulation domain was initialized using this vertical profile. The power law equation was used instead of the standard atmospheric logarithmic profile because in preliminary simulations it gave better results. The standard atmospheric logarithmic profile is shown in (28), with V_1 the velocity at a reference height z_1. Figure 10 compares the power law equation and logarithmic equation to the upstream profile data and shows that at heights above about 50 meters the data deviate significantly from the logarithmic profile and the power law equation fits better. The poor fit of the logarithmic profile above 50 meters may be due to a layer of non-neutral stability or it may be the top of the surface layer.

$$V(z) = 5.3792 z^{0.2113} \tag{27}$$

$$V(z) = V_1 \left[\frac{\ln\left(\frac{z}{z_0}\right)}{\ln\left(\frac{z_1}{z_0}\right)} \right] \tag{28}$$

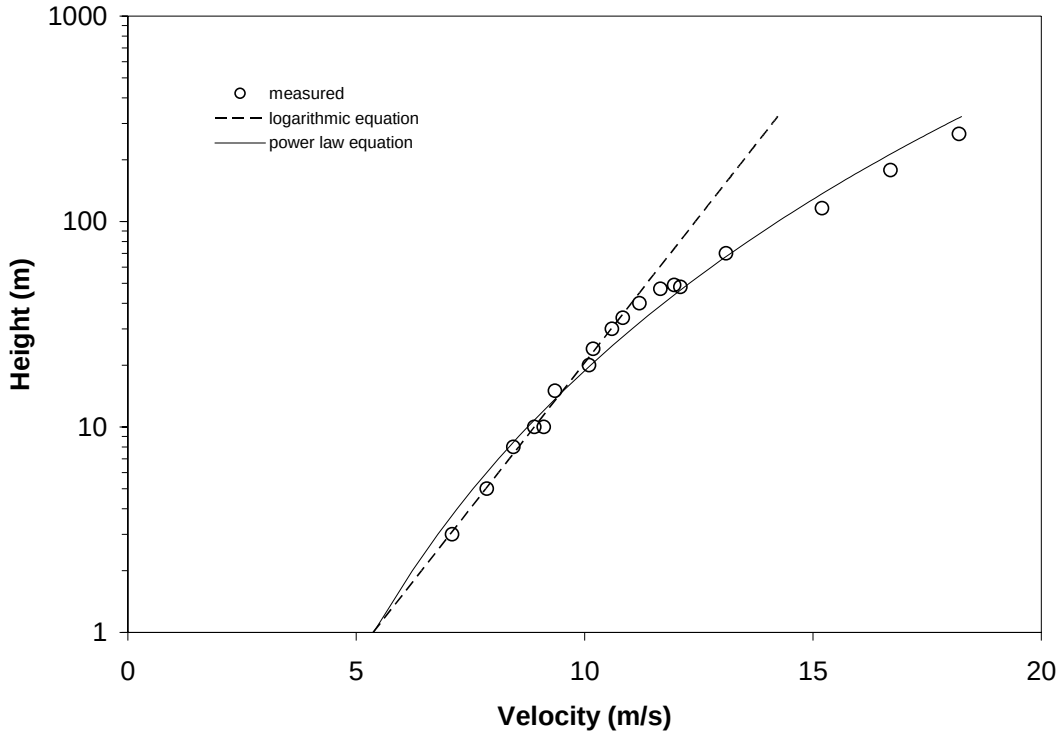

Figure 10. Comparison of wind velocities with a logarithmic and power law equation at the upstream reference site at Askervein Hill on semi-log axes.

A comparison of the base case simulation and the measured values along Lines A, AA, and B are shown in Figure 11. The simulation matches the measured data well, except on the lee side of the hill. Simulated values were within 15 percent of the measured values everywhere, except in the lee of the hill. Here, errors up to 150 percent were found. At the worst location, the measured value was 3.2 m/s compared to a simulated value of 8 m/s. The poor performance of the model on the lee side of the hill is most certainly related to momentum effects not incorporated in the model. Lopes (2003) found similar results for a mass-consistent model on Askervein Hill, and stated that this poor performance on the lee side was due to the kinematic nature of the model.

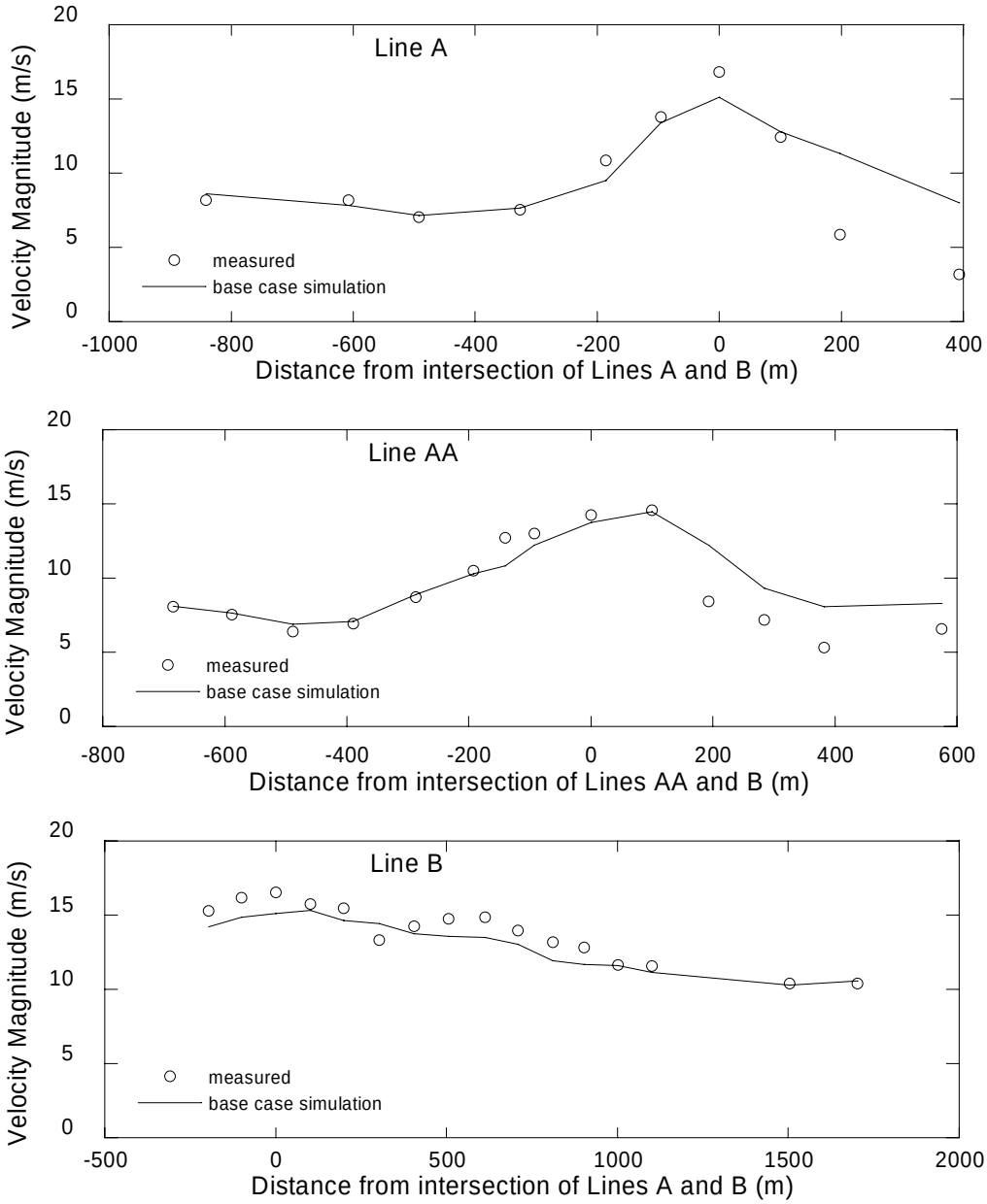

Figure 11. Comparison of measured wind velocity and base case simulation for Askervein Hill. Distances are in relation to reference lines identified in Figure 9.

3.3.1.1 Residual tolerance

The iteration residual tolerance is a measure of how close the current solution is to the actual numerical solution in the iteration process. Iterative solvers compute

successive solutions that, ideally, step closer and closer to the actual solution, down to the limitations of the computer's precision. The residual is a measure of the error between the current solution vector and the solution vector that solves the equation. The goal of the iterative solver is to reduce the residual vector to a small value. A method must be identified to decide when to stop the iterations when the error is small enough. For an $Ax = b$ system of n linear, algebraic equations in n unknowns, the residual, r, for iteration, i, is computed as

$$r^{(i)} = Ax^{(i)} - b \tag{29}$$

The stopping criteria used here is for the iterations to stop when

$$\left\| r^{(i)} \right\| \le stop\_tol \cdot \left(\left\| A \right\| \cdot \left\| x^{(i)} \right\| + \left\| b \right\| \right) \tag{30}$$

were $stop\_tol$ is a user specified value, and the norms are ∞ norms (Barrett *et al.* 1994).

A range of $stop\_tol$ values have been used to estimate when the error is small enough to stop iterating. The $stop\_tol$ values examined were: 0.001, 0.01, 0.1, and 1. Comparison of simulated velocities with the measured values along Lines A, AA, and B are shown in Figure 12. The values of wind speed are nearly identical for all simulations, except when $stop\_tol$ is 1. For this value, the solution vector is still changing and iterations should continue. Since values of 0.1, 0.01, and 0.001 give nearly identical wind speeds, significant reduction of the error is not gained by iterating to the smaller values. For these simulations, an adequate $stop\_tol$ is 0.1.

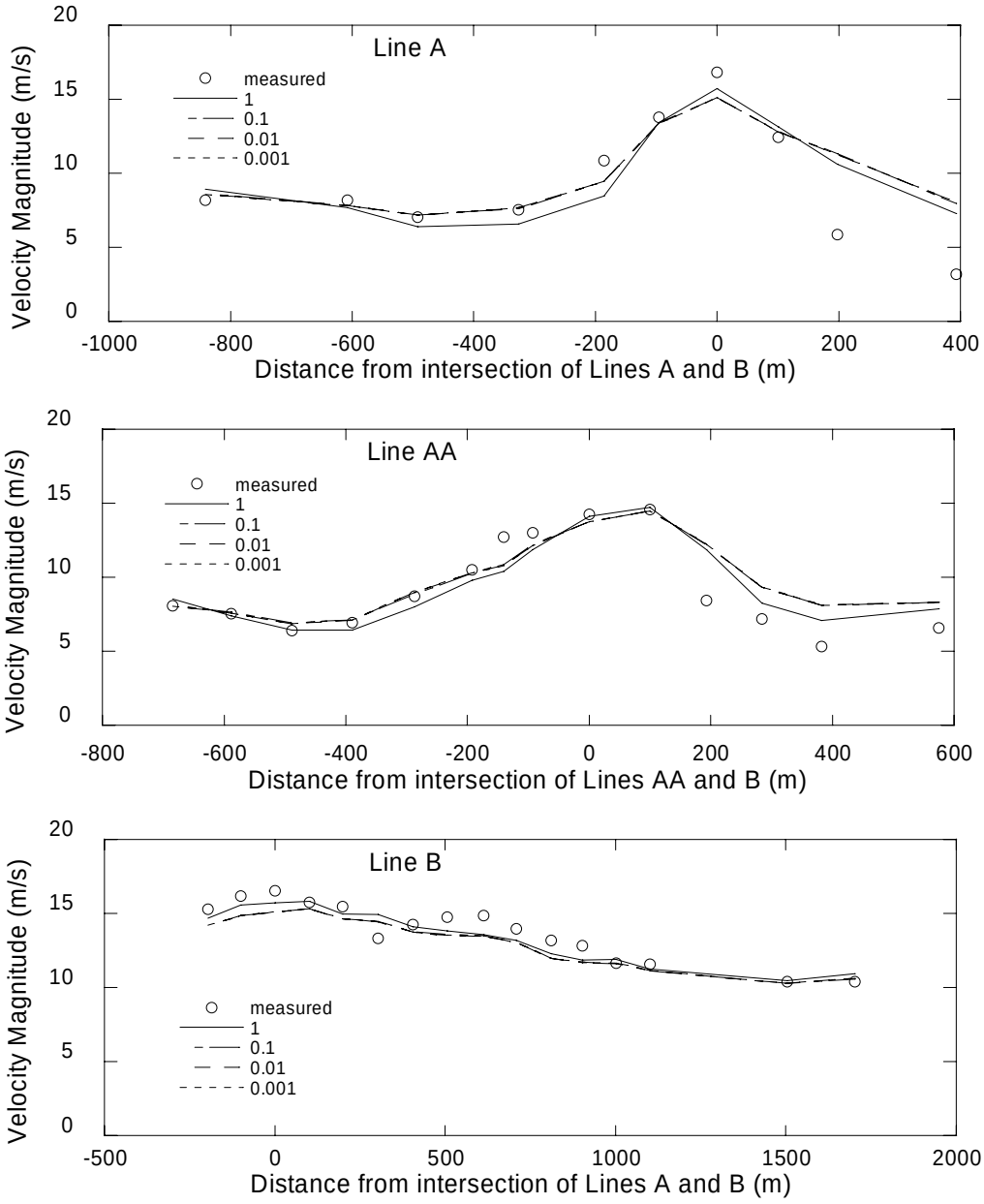

Figure 12. Comparison of simulated vs. measured wind velocities with different $stop\_tol$ values (equation (30)) for Askervein Hill. Distances are in relation to reference lines identified in Figure 9.

3.3.1.2 Quadrature point

When the governing elliptic partial differential equation (24) is rewritten in a weak form, volume integrals appear in the final finite element equation (25). The integration is performed numerically, element by element, using Gaussian quadrature

(see, for example, Thompson (2005)). In Gaussian quadrature, the more Gauss points used, typically the more accurate the integration. The downside is that using more Gauss points makes the simulation take longer.

The number of Gauss points used in the wind model was examined to determine how sensitive the output is to this parameter. This three dimensional model used 1, 8, and 27 Gauss points which corresponds to 1, 2, and 3 Gauss points in one dimensional integration. Comparison of the simulations to measured data is shown in Figure 13. As can be seen, no significant increase in accuracy is apparent with more Gauss points. So an appropriate number of Gauss points to use is 1.

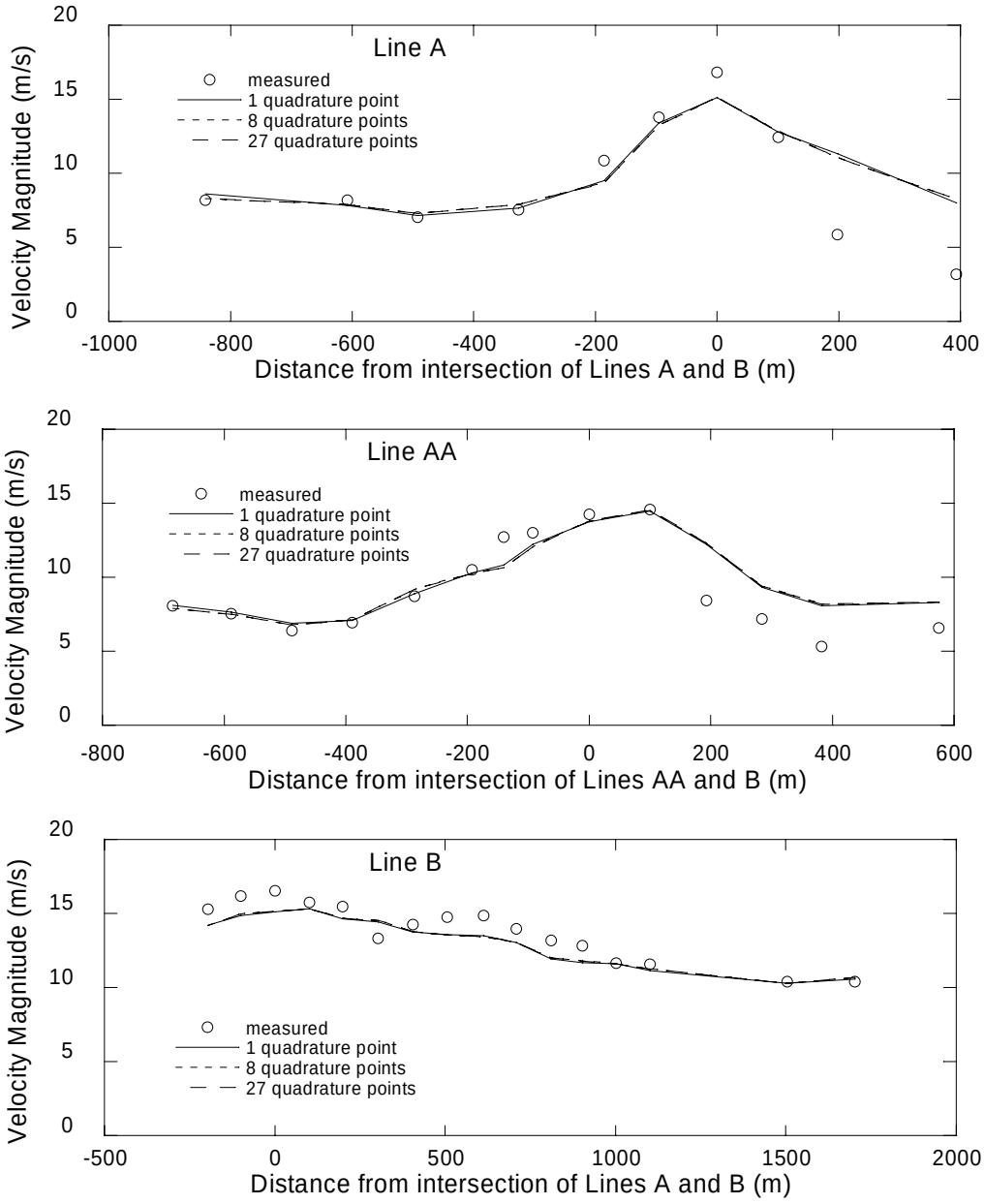

Figure 13. Comparison of simulated vs. measured wind velocities based on the number of quadrature points used in the numerical integration for Askervein Hill. Distances are from reference lines identified in Figure 9.

3.3.1.3 Horizontal resolution

The horizontal resolution used for the simulations was investigated. The values of horizontal cell size used were 23.4375, 40, 60, and 120 meters. Also, a simulation with a horizontal cell size of 120 meters with 27 point quadrature (rather than the base

case value of 1 point) was performed. This was done to determine if the accuracy of a low resolution simulation could be increased with more accurate numerical integration. The results of the simulations are shown in Figure 14. As can be seen, even the coarsest case of 120 meters produced results that compared reasonably well with the measured data. Again, simulated values were closer to measured values on the upstream side of the hill and at the top than on the lee side. The use of 27 point Gaussian quadrature for the 120 meter resolution case did not increase the accuracy. These simulations show that, for the terrain simulated, the solutions appear to be relatively insensitive to the meshes used. The 120 meter meshes may be beginning to diverge from the finer meshes, and so may have some artificial error due to the spatial discretisation. The 60 meter and finer simulations are probably insensitive to the mesh, at least compared to other inaccuracies in the modeling such as the incoming flow profile and atmospheric stability.

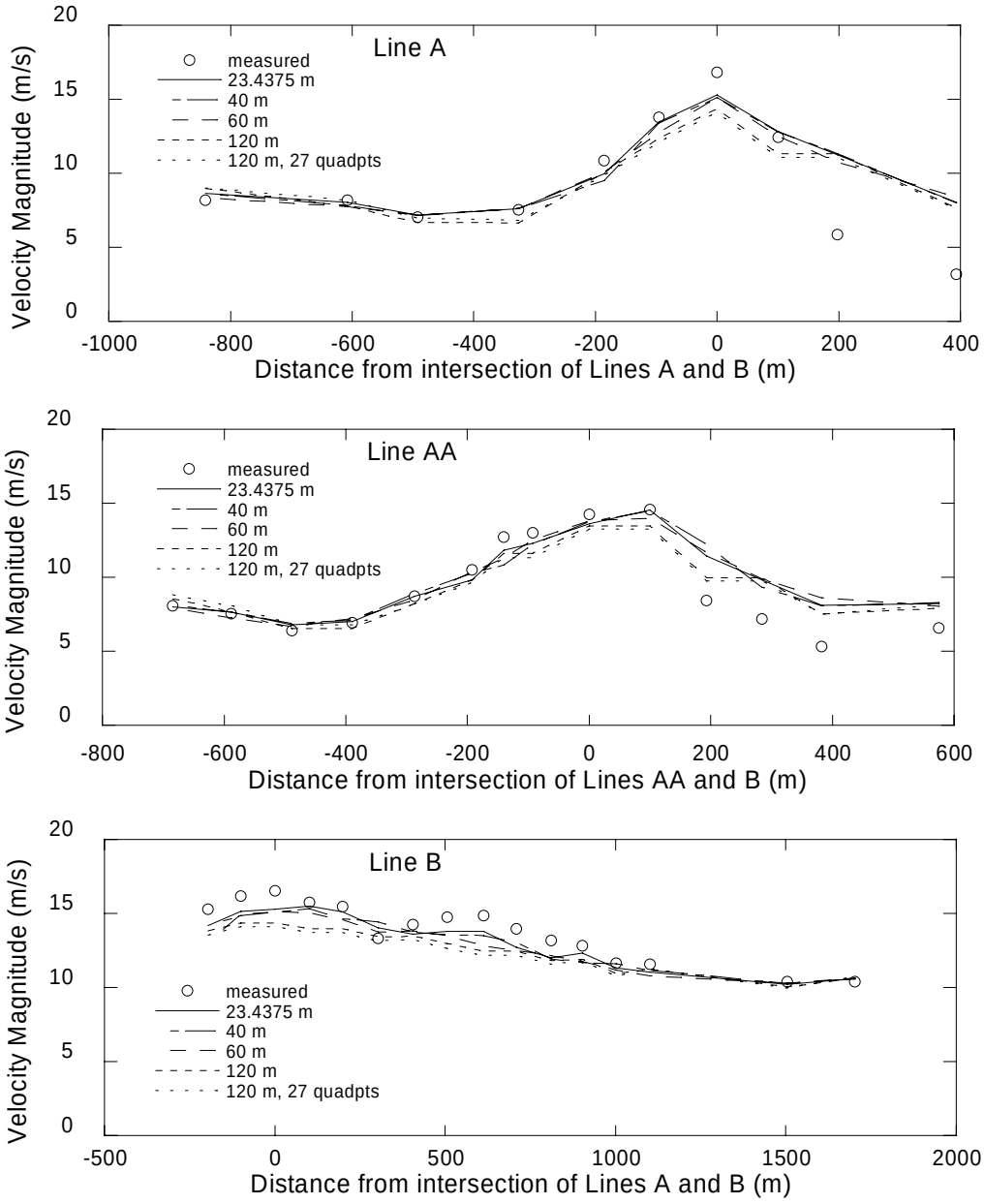

Figure 14. Comparison of simulated vs. measured wind velocities based on meshes with different horizontal cell resolution for Askervein Hill. Distances are in relation to reference lines identified in Figure 9.

3.3.1.4 Vertical resolution

The number of cells, or layers, in the vertical direction was examined. In this direction, the cell size increases with height above the ground so that the cells are clustered near the ground where the largest gradients are found. In all simulations

compared in this section, the cells grow vertically at a rate of 30%. That is, a cell is 30% larger in the vertical direction than the one immediately below it. Figure 15 shows the simulations of 15, 20, 30, and 35 vertical cells. The 15 and 20 layer simulations were identical and gave reasonable results. The 30 and 35 layer simulations were significantly different from the 15 and 20 layer simulations and the measured data. The simulations appear to show a trend of less accuracy with more cells in the vertical direction. This goes against intuition, which would predict better or equal accuracy with higher resolution. It was hypothesized that this problem was not that of the vertical resolution, but something else related to vertical resolution. The next section offers a probable explanation: the cell aspect ratio.

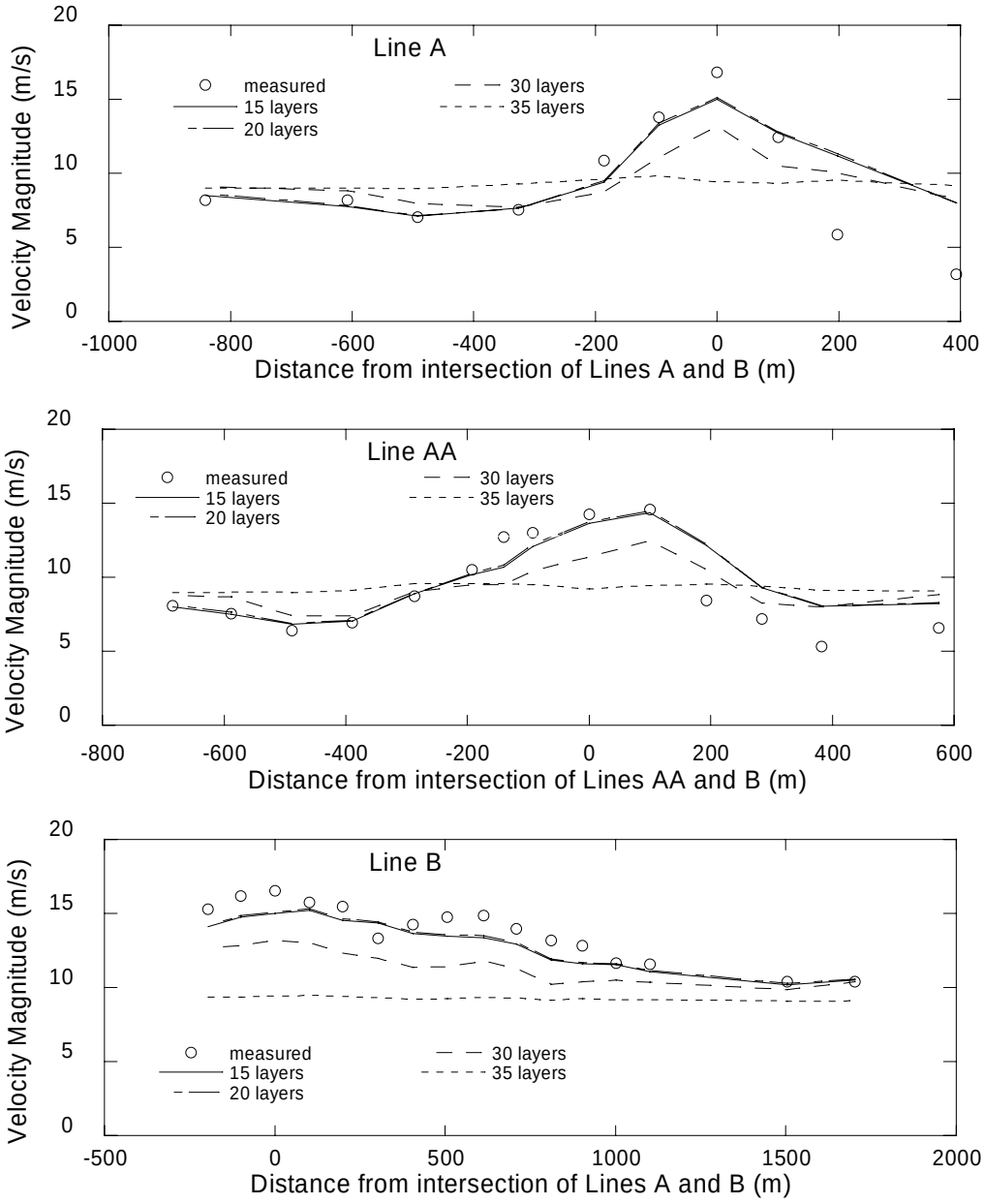

Figure 15. Comparison of simulated vs. measured wind velocities based on meshes with different numbers of vertical layers of cells for Askervein Hill. Distances are in relation to reference lines identified in Figure 9.

3.3.1.5 Cell aspect ratio

The cell aspect ratio is a measure of the relative difference between the minimum and maximum edge lengths of a cell. The cell aspect ratio is computed from (31) and (32). The n direction in (32) refers to the two horizontal directions and

the vertical direction. It is the actual edge length, not the projected edge length in the given direction. In the finite element method, excessively large aspect ratios can lead to numerical problems. Reasons for these problems can include interpolation accuracy, discretisation error, and poor condition number of the global stiffness matrix. The value of aspect ratio above which poor results are obtained varies. It depends on the partial differential equations being solved, the shape functions, and the kind of element, to name a few.

$$Q_{AR} = \frac{\max(e_1, e_2, e_3)}{\min(e_1, e_2, e_3)} \quad (31)$$

$$e_n = \frac{\sum edge\ lengths\ in\ n\ direction}{number\ of\ edges} \quad (32)$$

In the model, aspect ratio is not a direct input, but rather a result of the horizontal cell size, number of vertical layers, vertical layer growth, height of the domain, and the terrain. These parameters determine the size and shape of the elements as well as the aspect ratio.

An example of the possible problems that can be encountered when too high of an aspect ratio is used is shown in Figure 16. The parameters used in the two simulations are shown in Table 3. For the two simulations, the mesh was deliberately made to have very flat, “pancake-like” cells that had high aspect ratios of 590 and 983. As seen in Figure 16, the mesh with an aspect ratio of 983 gave an unrealistic flow field, but the mesh with a 590 aspect ratio gave a realistic flow field. For these simulations, the only parameter that was changed the horizontal cell size. Other simulations, not shown here, also support the idea that high cell aspect ratios can be responsible for poor model performance. To avoid problems, it appears that cells

should have aspect ratios less than 600. A more conservative number, which is recommended here, is to have aspect ratios less than 400.

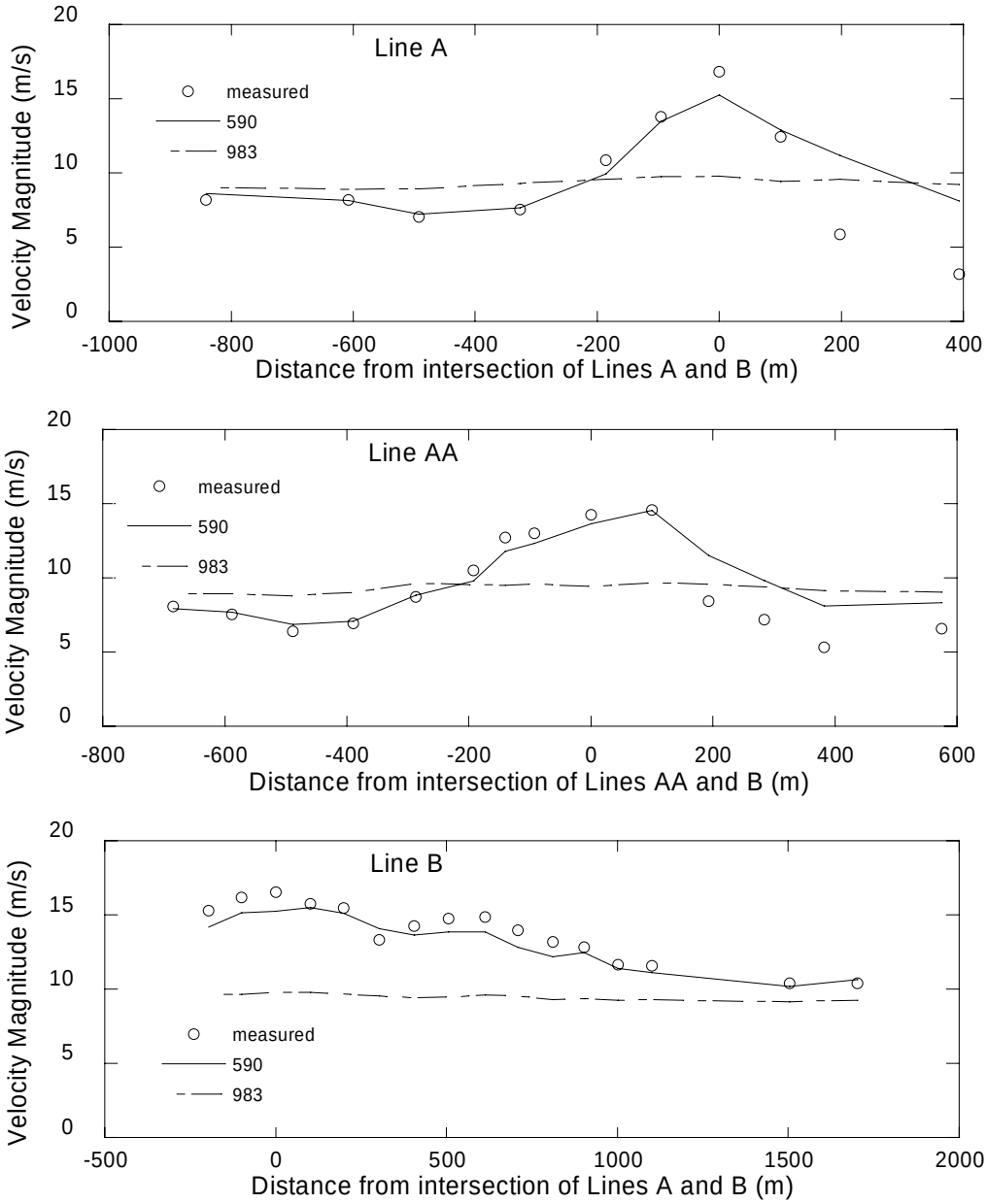

Figure 16. Comparison of simulated vs. measured wind velocities based on meshes with different aspect ratio (equation (31)) for Askervein Hill. The case with an aspect ratio of 590 used the same input parameters as the 983 aspect ratio case, except that the horizontal cell size used was 23.4375 meters instead of 40 meters which gave the lower aspect ratio. The vertical cell sizes were approximately equal. Distances are in relation to reference lines identified in Figure 9.

Table 3. Parameters used for 2 simulations comparing the effect of aspect ratios (equation (31)) for Askervein Hill.

Resulting aspect ratio	# vertical layers	Vertical cell growth	Horizontal cell size	Resulting vertical cell height
590	20	65%	23.4375	0.04
983	20	65%	40	0.04

3.3.2 Waterworks Hill

In July of 2004, the Missoula Fire Sciences Laboratory measured wind speeds over a hill near Missoula, MT named Waterworks Hill (Bradshaw 2004). The hill is approximately 200 meters tall and has a relatively flat upwind fetch to the West of over 10 kilometers. To the North, East, and South the hill is surrounded by larger hills and mountains. It is covered with grass that is approximately 8-30 centimeters tall. The measurements were taken to provide a full scale data set to aid in wind model validation. Simulations from the model described in this paper will be compared to the measured data.

During the Waterworks Hill measurement campaign, a total of 9 wind measurement towers provided data. Ten towers 3.05 meters (10 feet) tall were temporarily placed on the hill, but problems with 3 resulted in only 7 providing usable data. An additional, existing wind tower in the drainage to the East of the hill was used. This tower was called the “Tulip tower” and also measured winds at 3.05 meters (10 feet). The last tower is operated by the National Weather Service and located at the Missoula Airport. This station is approximately 8 kilometers to the West-Northwest of the hill and measures winds at 10 meters above the ground. The wind measurement period was during a cold front passage that was characterized by strong winds for this

area. For a period of 3 hours, hourly averaged wind speeds at the Missoula Airport were consistently between 9.4 m/s and 10.3 m/s from the West.

The elevation data used in the simulations were obtained from the USGS (USGS 2006). The elevation data was 30 meter resolution raster data. The domain size used was approximately 21 kilometers by 16 kilometers and is shown in Figure 17. The top boundary of the computational domain was 5 kilometers above sea level.

Figure 17. Topography map of Waterworks Hill and surrounding area. North is toward the top of the image. The black triangles represent locations of wind measurement towers. The West most tower is the Missoula Airport tower and the East most tower is the Tulip tower. The other 10 towers are located on the actual hill. The elevation contour interval is 20 meters.

The National Weather Service weather station at the airport was used to initialize the flow domain for the simulations performed. Since this is a surface wind measurement with no wind profile information, an estimate of the velocity profile was made. Because the winds were strong and the atmosphere was well mixed, a

logarithmic velocity profile (28) was used as the estimated profile. The roughness length, z_0, was 0.02 meters which corresponds to low grass in the area (Wierenga 1993). The reference velocity used in the logarithmic profile to initialize the flow domain was adjusted until it gave a simulated flow field that matched the velocity measured at the National Weather Service weather station. This reference velocity was 8.6 m/s at 3.048 meters above the ground. The value measured at the National Weather Service weather station was 9.8 m/s from 270 degrees at a height of 10 meters.

Four simulations with differing mesh characteristics were performed. The parameters and resulting aspect ratios for these meshes are shown in Table 4. The finest grid is grid 1 and the coarsest grid is grid 2. All simulations used a vertical cell growth of 30%, single quadrature point integration, and iterated to a $stop\_tol$ value of 0.1.

Table 4. Mesh parameters for the Waterworks Hill simulations.

	Number of vertical cells	Horizontal cell size (m)	Largest aspect ratio
grid 1	30	50	157
grid 2	30	60	166
grid 3	30	100	288
grid 4	20	200	37

Wind vector plots of the four simulations are shown in Figure 18. Figure 19 shows the results of the four simulations compared to the measured data. The diagonal line through the plot is the line of perfect agreement. From this figure, it is evident that a mesh insensitive solution has probably not been reached. There are still differences of up to 28 percent between the finest grid, grid 1, and the next finest grid, grid 2. Limitations in computer memory did not allow simulations with finer grids. The

computer memory and CPU times are shown in Table 5. In discussing CFD meshes, Stangroom (2004) states that true grid independence is unlikely to be achieved in wind engineering problems, but that useful information on mesh sensitivity can be obtained. This sensitivity analysis gives an estimate of the spatial discretisation errors in the solution. In the Waterworks Hill simulations, these errors likely could be in the 20-30 percent range.

Table 5. Computing requirements for the Waterworks Hill simulations.

	memory (MB)	CPU time (s)
grid 1	1500	1462
grid 2	1221	1176
grid 3	437	412
grid 4	72	13

The results in Figure 19 show that, for the higher wind speeds, the simulations consistently under-predicted the velocity. These higher wind speed stations were located near the top of the hill. For the other stations, a consistent under-prediction is not evident. A possible reason for this under-prediction would be that the assumed logarithmic vertical velocity profile did not approximate the real atmosphere well. Actual velocities high above the ground could have been stronger than the logarithmic profile predicted.

All simulations over-predicted the winds at the Tulip tower, with Grids 2 and 3 having the largest errors of 54 % and 52 %. This tower is located at the bottom of a drainage to the East of Waterworks Hill, in an area of scattered trees and buildings. Since the wind simulations assumed a ground roughness of grass everywhere, it is possible that the scattered trees and buildings here sheltered the tower giving lower wind speeds. If this were the case, the Tulip tower data may be suspect. Another

possibility for the over-prediction is that momentum effects on the lee of the hill produced the measured low wind speeds. As discussed for Askervein Hill, these momentum effects are not accounted for in the model and so the model would predict higher velocities.

Table 6 compares the largest error in simulated velocities for each grid, with and without the Tulip tower. Grids 2 and 3 show improvement when the Tulip tower is not included. Also shown in Table 6 is a comparison of the correlation coefficients for the different simulations (includes the Tulip tower data). As expected, the finer grids correlate better with the measured data than the coarser grids.

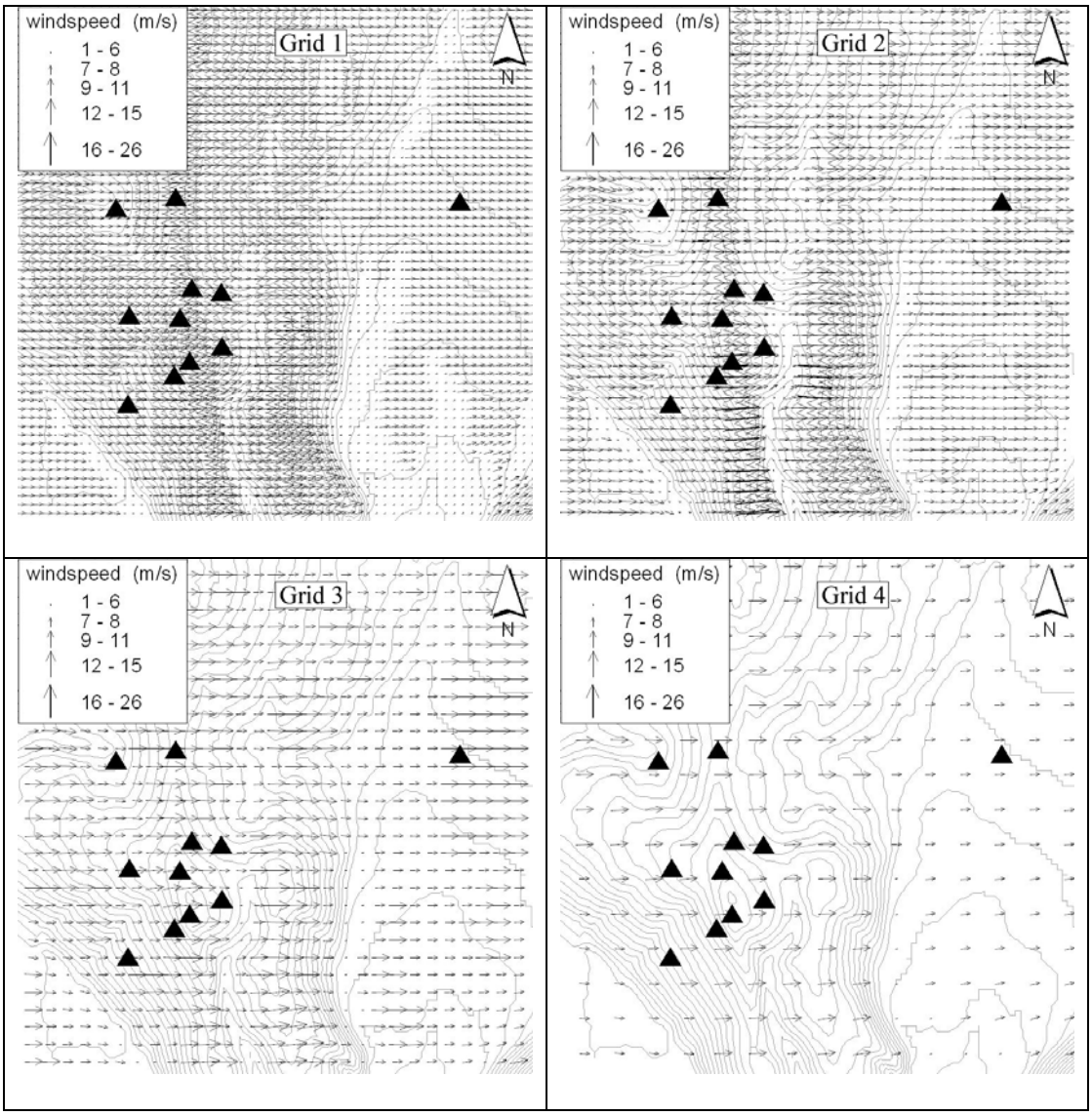

Figure 18. Wind vectors on Waterworks Hill for different grids. The plots are zoomed in to the hill area. Measurement stations are shown as black triangles.

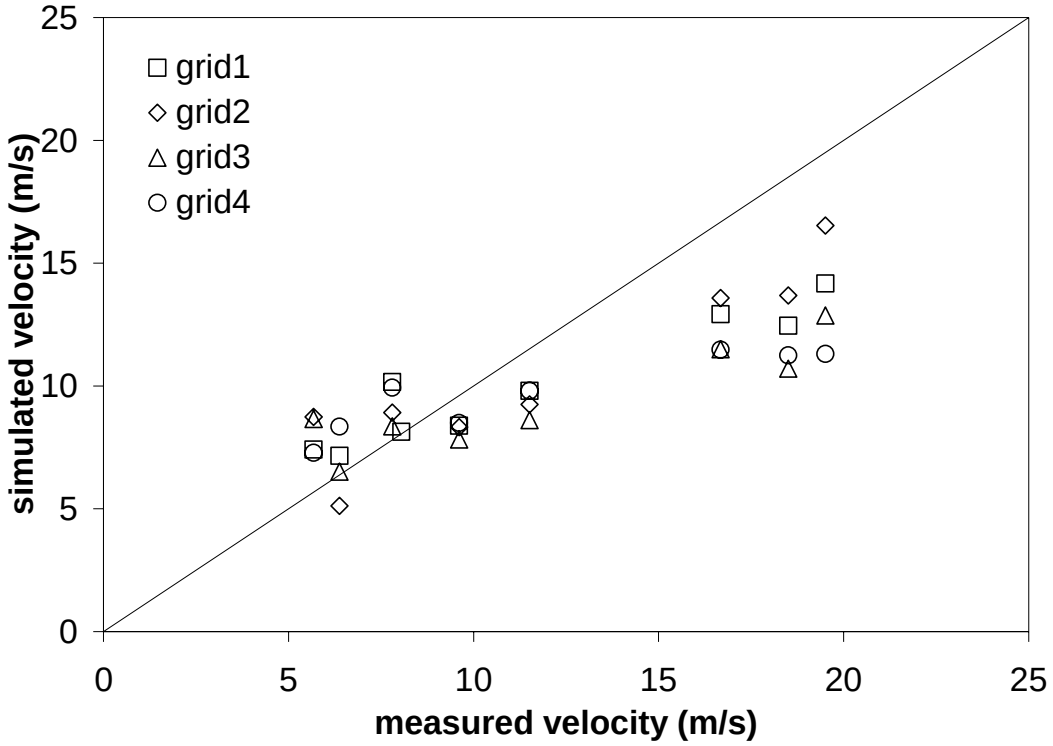

Figure 19. Waterworks Hill simulation results compared to measured values.

Table 6. Error and correlation comparison for Waterworks Hill simulations.

	largest error in windspeed (%)	largest error in windspeed w/o Tulip station (%)	simulation correlation
grid 1	32.69	32.69	0.943
grid 2	54.02	26.00	0.929
grid 3	52.50	42.15	0.899
grid 4	42.05	42.05	0.903

3.4 Conclusions

The mathematical model has been described, and simulations for two full scale field experiments were completed. A sensitivity analysis was done for some of the numerical input parameters. It showed that aspect ratios larger than 600 give very poor results and a more conservative limit to use might be 400. Another important result is that simulations are insensitive to the number of quadrature points used in the

numerical integration. Single point quadrature can be used to reduce computational time. Guidelines for other parameters such as when to stop the iterative solver were found.

Comparison to the measured data showed that the model is capable of producing flow fields within about 30 % of measured values in many cases. This appears to be true for areas other than the lee side of hills. On the lee side of hills the model gave larger errors of up to 150 %. This problem is probably due to the model not explicitly incorporating a momentum equation.

Nonetheless, the model produced wind fields that compared well enough with the measured data to probably be of use to fire managers. Simulations in steeper, more rugged terrain that some fires burn in would be expected to give less impressive results. However, as also concluded by Lopes (2003), numerical tools such as the one described should at least give fire managers information on the relative wind characteristics of different locations in terrain for fire management purposes.

CHAPTER 4. FIRE SPREAD SIMULATIONS

4.1 Introduction

Fire plays an important role in the environment. Many ecosystems have evolved with fire as an integral, necessary process. In fact, exclusion of fire can have detrimental effects that significantly change the ecosystem (Arno and Brown 1991). Nevertheless, wildland fires can also have very destructive and unwanted effects on society including loss of property and life. Land managers are faced with making difficult decisions about how to best balance conflicting goals. Prediction of fire behavior is often used in making these decisions.

The prediction of fire behavior requires accurate knowledge of the factors affecting the fire. These factors can be grouped into three categories: fuels, weather, and topography. Weather is often the dominating influence, and in particular the wind. A fire burning in calm winds can dramatically change character when exposed to high winds. The relation between wind speed and spread rate is nonlinear such that a change in wind speed can produce a larger change in spread rate (Rothermel 1972). What compounds this even more is that wind often fluctuates on relatively small temporal and spatial scales. These variations can be much smaller than the scale of a large fire so significant differences can be seen across the fire. Error in fire predictions

can come from inadequate descriptions of these winds. Surprisingly, few authors have described methods of simulating wind for application to wildland fire behavior. Possible reasons include: the complex nature of the phenomena, including turbulence and nonlinear effects; the computational requirements and the time constraints associated with wildland fire; and the relatively small amount of research and funding for work at this scale compared to the weather prediction or industrial (automotive, aerospace, etc.) scales.

The most widely used spatial wildland fire spread model is FARSITE (Finney 1998). The typical incorporation of wind in FARSITE is to assume that the wind speed and direction do not vary spatially over the modeling domain (although they can vary temporally). In many cases, this is a poor description of the wind field. FARSITE has the ability to incorporate gridded (or spatially changing) wind fields, yet this has not been utilized in the past because of the lack of a model to produce the wind fields.

The current study will assess the use of two models to produce gridded wind fields for use in FARSITE. Comparisons of fire spread will be made using the new gridded wind models and the traditional method of a spatially uniform wind field. These comparisons will be done for three fires. One is a hypothetical fire spreading over a low hill that has detailed wind information available from a field study (Taylor and Teunissen 1983; Taylor and Teunissen 1985). The other two are historic fires that resulted in firefighter entrapments and/or fatalities: South Canyon Fire (Butler *et al.* 1998) and Mann Gulch Fire (Rothermel 1993).

4.2 Background Modeling Discussion

Modeling the spread of a wildland fire is difficult because of the complex physical mechanisms involved. The most useful models so far (in an operational sense) are relatively simple (Rothermel 1972; Van Wagner 1977), using parameterizations of heat transfer, fluid flow, and chemical reactions developed from experimental work. They are generally termed empirical or semi-empirical models. The main advantages of these models are that they are simple to understand, can be computed quickly on a computer (Andrews 1986; Finney 1998), and often describe the gross behavior of a fire well. Other more physically based models have been developed (Clark *et al.* 1996; Grishin 1997; Linn 1997; Mell *et al.* 2007; Porterie *et al.* 2000). They include so called coupling effects of fire generated buoyancy on the surrounding fluid flow as well as detailed treatment of heat transfer. In theory, these models should be more robust than the simpler models. However, they suffer from long computer run times, often complex data requirements, and are generally not validated. For these reasons, they are not currently used operationally on fires.

A possible solution to bridge the gap between the simple and more complex models is to simulate the wind near the ground surface without the coupling effects from the fire. Such a model would move a step closer to the more physically based models, yet allow the use of the current semi-empirical fire spread models. It has also been shown to be feasible under operational time constraints (Forthofer *et al.* 2003). The combination may improve the accuracy of fire simulations since a better description of the wind would be used.

Several models have been developed to predict wind. They can be classified into either prognostic or diagnostic models. The prognostic models step forward in time from an initial wind field while the diagnostic models simulate one instant in time (sometimes called steady-state models). Most prognostic models have been developed for weather prediction at scales larger than fires. Cell resolutions of 36, 12, or 4 kilometers are common. This scale difference can limit their use on wildland fires. For example, a 100,000 acre fire is about 11 km in diameter if it has a circular shape. This means that, at best, only a few cells span the fire area which probably does not warrant using a spatially varying description. Also, because of their resolution, most weather models were not developed to resolve the winds modified by individual ridges, valleys and mountains. Rather they hope to approximate the effects of larger features such as mountain ranges. In effect, the coarse weather models smooth over the small scale features because of their large cell sizes. In many cases, these small scale features have a great influence on the local winds influencing a fire and should be considered. Also, these prognostic models have high computing requirements, generally requiring multi-processor computers which also limit operational use. In contrast, the diagnostic models typically have relatively small computer requirements (from minutes to a couple of hours per run on a single processor computer). The penalty for this speed up is incorporation of less physics and a wind field for only one instant in time.

Among the diagnostic models is a range of modeled physics. Some only incorporate the conservation of mass (Chan and Sugiyama 1997; Davis *et al.* 1984; Geai 1987; Montero *et al.* 1998; Moussiopoulos and Flassak 1986; Ross *et al.* 1988;

Sherman 1978). These models generally give a poor estimation of winds on the lee side of hills due to momentum effects that are not incorporated. Other models include the conservation of mass and momentum (Alm and Nygaard 1995; Lopes 2003; Raithby and Stubley 1987; Uchida and Ohya 1999). These models have compared well to data in cases of isolated hills in neutral stable atmospheric conditions. Lastly, some models incorporate conservation of mass, momentum, and energy (Apsley and Castro 1997; Montavon 1998). They have been shown to simulate wind in stable and neutral atmospheric conditions well. All of the diagnostic models are designed to model the effect of topography on wind flow.

This study examines wind predicted with two different types of diagnostic models. One is a commercial computational fluid dynamics model (Fluent®) incorporating the conservation of mass and momentum (described in Chapter 1). The other is a mass conserving model (described in Chapter 2). Both assume neutral atmospheric stability. Byram and Nelson (1974) state that most large wildfires occur when the atmosphere is nearly neutral so a model incorporating these physics seems reasonable. Models incorporating the conservation of energy are more robust for non-neutral atmospheric conditions but have the disadvantage of more complex and sometimes difficult to obtain inputs and longer computing times. Neglecting conservation of energy greatly simplifies the model.

Although diagnostic wind models are prolific in other fields such as wind power generation and dispersion of pollution, there are comparatively few instances in fire prediction. These few studies have shown that the use of gridded wind can improve fire spread predictions in mountainous terrain. Lopes (2002) developed

FireStation which combined two wind models, very similar to those described here, and a spatial fire spread model. The fire spread model was cellular based and the wind models were a strictly mass conserving model and a mass/momentum conserving model. A thorough assessment of the effect of the wind models on the fire spread is not done. A historic fire is simulated and compared to a reconstructed perimeter with good agreement. However, only one simulation is shown, and the author does not state which wind model was used for the simulation. No comparison is made between fire simulations using the two different wind models or with a uniform wind field. Since its development FireStation has not seen widespread use operationally, possibly because of deficiencies in the cellular based fire spread model.

Forthofer et al. (2003) and Butler et al. (2004) describe preliminary results of the work described here. A mass and momentum conserving wind model is used in conjunction with a wave propagation fire spread model (Finney 1998). In all cases, using the winds provided by the diagnostic wind model improved the fire spread predictions when compared to a simulation using a uniform wind field.

4.3 Models

The fire model used in this study was FARSITE (Finney 1998). Two different wind models are used: a mass-consistent model and a mass and momentum conserving CFD (computational fluid dynamics) model. Since the wind modeling does not incorporate any effects the fire has on the wind, the two models can be run independently. Information transfer between the wind models and fire model occurs via text files written to the hard drive. These text files are written by custom utility programs.

4.3.1 Fire Spread Model

FARSITE incorporates models of surface fire, crown fire, point-source fire acceleration, spotting, and fuel moisture. Fire spread in two dimensions is accomplished using a one dimensional spread rate model and the assumption of an elliptical 2-dimensional fire shape. The eccentricity of the assumed ellipse is a function of the effective wind speed. The fire perimeter is tracked using a vector technique (Huygen's principle). Minimum spatial input themes needed by the model are elevation, slope, aspect, fuel model and canopy cover. Other required inputs include temporal weather data, fuel moisture information, numerical simulation parameters, and ignition locations.

Users have two options for wind input. The standard selection is to use uniform, non-spatial winds in the form of a FARSITE .wnd file. This file must contain wind speed, wind direction, and cloud cover values for discrete times spanning the simulation duration. These values are applied across the entire landscape. The other option is to use a spatially varying wind field. In FARSITE, this is called "gridded wind". An .atm file is constructed that lists velocity, direction and cloud cover file names for discrete time segments that span the simulation duration. This way, different wind fields can be used at different times during the simulation. The velocity, direction, and cloud cover files describe the spatial distribution of these values in a raster-type format. The .atm file replaces the usual .wnd input file in FARSITE. The separate gridded velocity, direction and cloud cover files listed in the .atm file must be located in the same directory as the .atm file. Their format is ASCII raster, the same as the other spatial input files used by FARSITE. If cloud cover is not simulated in the

gridded wind model, a uniform valued gridded file can be used. Current restrictions in FARSITE are that each gridded theme (velocity, direction, and cloud cover) must separately have the same resolution and spatial extent. For example, all velocity and direction files could be of one resolution and extent, while cloud cover could be completely different resolution and extent. Another restriction in FARSITE is that the .atm file must include at least one entry of wind and cloud cover per day during the simulation. Additional information on using gridded wind can be found in the FARSITE help menu (Finney 1998).

4.3.2 CFD Wind Model

The CFD wind model is a general purpose, multidimensional, computational fluid dynamics code called FLUENT®. CFD was developed primarily to model flows of interest in industrial applications. Recently, CFD has gained popularity in wind engineering applications such as wind energy assessment and pollution dispersion. The settings in FLUENT® can be adjusted to simulate an atmospheric boundary layer. A detailed description of the CFD model can be found in Chapter 1.

The flow domain was discretized using a finite volume approach. Air was modeled as an incompressible fluid and the Coriolis effect neglected. Turbulence closure of the flow equations was simulated by the RNG k-ε model (Yakhot and Orszag 1986). In a study of turbulence models for neutral stable atmospheric applications, Kim and Patel (2000) found that the RNG k-ε model gave the best agreement with experimental data. The SIMPLEC solver (Vandoormaal and Raithby 1984) was used on an unstructured grid. At inlet boundaries, uniform flow conditions were specified. The fire area was placed far enough downstream so that a boundary

layer would develop before reaching the fire location. At the ground, a wall function boundary condition was used. Appropriate roughness parameters for vegetation were obtained from Wierenga (1993). Files of velocity and direction were written for use in FARSITE and a GIS. Wind simulations took approximately 0.5-1.5 hours on a modern, single processor computer.

A separate code called GAMBIT® was used to build the computational mesh used in FLUENT®. A digital elevation model (DEM) file was read and converted to a GAMBIT® specific format through a custom utility code. A hybrid unstructured mesh was built in GAMBIT® with several layers of wedge cells growing vertically from the ground followed by generation of vertically growing tetrahedral cells above the wedge cells. The resulting mesh clustered most cells near the ground where the largest flow gradients occur, yet minimized the cell count to reduce computation times. The near ground wedge cell layers reduce numerical diffusion that can occur with other cell types.

4.3.3 Mass-consistent Wind Model

The mass-consistent wind model used here minimizes the change from an initial wind field while strictly conserving mass. The governing elliptic partial differential equation was solved numerically. A finite element discretisation technique was used in conjunction with a simple hexahedral cell mesh. A Jacobi preconditioned conjugate gradient solver was used to solve the set of linear, algebraic equations. Wind simulations take approximately 1-15 minutes on a modern, single processor computer. In all simulations performed here, the modeling domain has been initialized using one wind speed and direction at a specified height above the ground. The domain is filled

vertically assuming a neutral stable logarithmic wind profile and a roughness height for the dominant vegetation in the area (Wierenga 1993). The modeling domain is larger than the fire area to reduce any boundary condition effects. Files of velocity and direction are written for use in FARSITE and a GIS. More detailed information about the mass-consistent model can be found in Chapter 2.

4.4 Case Studies

Three different fire scenarios were simulated. One of the fires was a hypothetical fire burning over a real hill. This site was selected because detailed wind measurements were available for this hill. The simulations of wind flow and fire spread over the hill highlight some of the primary differences between the wind fields used. It also shows some of the sensitivity of the fire spread model to these simulated wind fields. The other two fires are historic fires that resulted in firefighter fatalities. They were selected because published investigations were carried out on these fires that included relevant weather and fire behavior information. For one of the fires, detailed fire spread information was available. Fire growth was simulated using different wind field scenarios obtained from the wind models discussed above. The fire growth simulations were compared to fire behavior reconstructed from witness accounts. For all of the case studies, three different wind field scenarios are used in the fire spread model: 1) The wind fields are from the mass-consistent model, 2) wind fields from the CFD model, 3) spatially uniform winds.

For the historic fire with fire perimeter information available, two different methods of comparing the simulated fire perimeters with the observed values have been used. The first is to visually compare the perimeters. This gives a qualitative

measure of how close the simulated perimeter is to the observed. Finney (2000) states that this method of comparison is most often used (Anderson *et al.* 1982; Coleman and Sullivan 1996; Finney 1994; Finney 1995; Sanderlin and Van Gelder 1977; Xu and Lathrop 1994). Although subjective, this method can give insight into modeling accuracy. Using this method, the level of agreement is usually readily understood.

The second method of comparison is more objective. It involves computing the simulated area that overlaps, under-predicts, and over-predicts the observed fire perimeter at a single time during the fire's progression. This method was used by Churchill (2001). The method used here reports the three areas as percent of total measured area to allow easier comparison. A disadvantage of this method is that there are three measures of fit for each simulation (overlap, under-prediction, and over-prediction) rather than one, as in for example an R^2 measure of fit. This can make comparisons of different simulations more complicated. A single measure of fit could not be found that performs acceptably. Methods to objectively compare measured and simulated fire perimeters are discussed by Finney (2000), but no techniques could be found that adequately reflect the space and time dependent trends of the fire growth patterns.

Comparison of model simulations to observed fire perimeters is done here to suggest differences between the wind fields used and the wind models that produced them (CFD, mass-consistent, uniform). It is not possible to "validate" the models (combinations of fire and wind models here) since the error of the input data or observed data used for comparison are not controlled or known (Rykiel 1996). Input values such as fuels and weather information as well as the measured fire behavior

have an unknown amount of error. In the absence of controlled error for these inputs and observations, the results of any comparison cannot be interpreted as to the cause(s). Finney (2000) and Albini and Anderson (1982) both conclude that full validation of FARSITE and the Rothermel spread equations, respectively, is not possible.

Although the fire simulations cannot fully validate the methods used here, the relative effectiveness of the three different types of wind fields is evaluated within the context of fire growth simulation accuracy.

4.4.1 Askervein Hill

Fire spread over a low hill has been simulated to compare the differences between the three different types of wind fields. The hill is a real hill, called Askervein Hill, that was the site of a large wind measurement study (Taylor and Teunissen 1983; Taylor and Teunissen 1985). Figure 20 shows the hill area, including Lines A, AA, and B along which wind measurement devices were placed. Simulations of wind flow over Askervein hill from the CFD and mass-consistent wind models have been compared with the wind measurements (Chapters 1 and 2). As seen in Figure 21, comparisons showed that both models do a very good job predicting the wind on the upwind side of the hill and at the top. On the lee side of the hill, the CFD model did a much better job predicting the wind pattern than the mass-consistent model. The differences between the wind models on the lee side of the hill are probably due to the included physics in the models.

Although a real fire did not burn over Askervein Hill, hypothetical fires have been simulated to show the differences in fire spread that can occur with different types of wind fields. The knowledge of the accuracy of the simulated wind fields for

Askervein Hill will give credibility to the simulations. Three fire simulations were done, holding everything constant except the wind field. The winds used were a uniform field, a CFD simulated field, and a mass-consistent simulated field. The fuel and other weather conditions used are shown in Table 7. The hypothetical fire was ignited upwind of Askervein Hill as a point ignition and allowed to spread for three hours. For the uniform wind simulation, a velocity of 18 mph at 20 feet above the ground was used. This is the same velocity as the CFD and mass-consistent wind fields upwind of the hill.

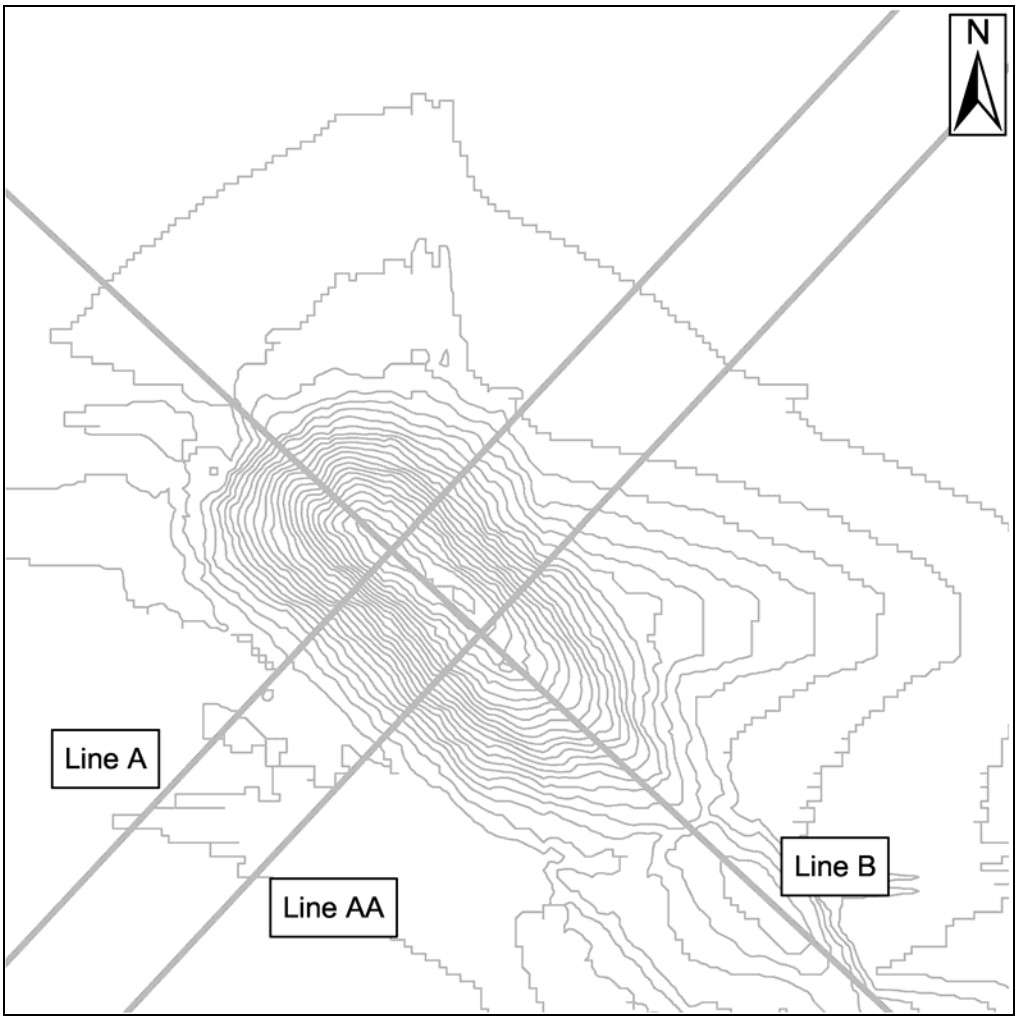

Figure 20. Contour map of Askervein Hill showing locations of Lines A, AA, and B. The contour interval is 5 meters.

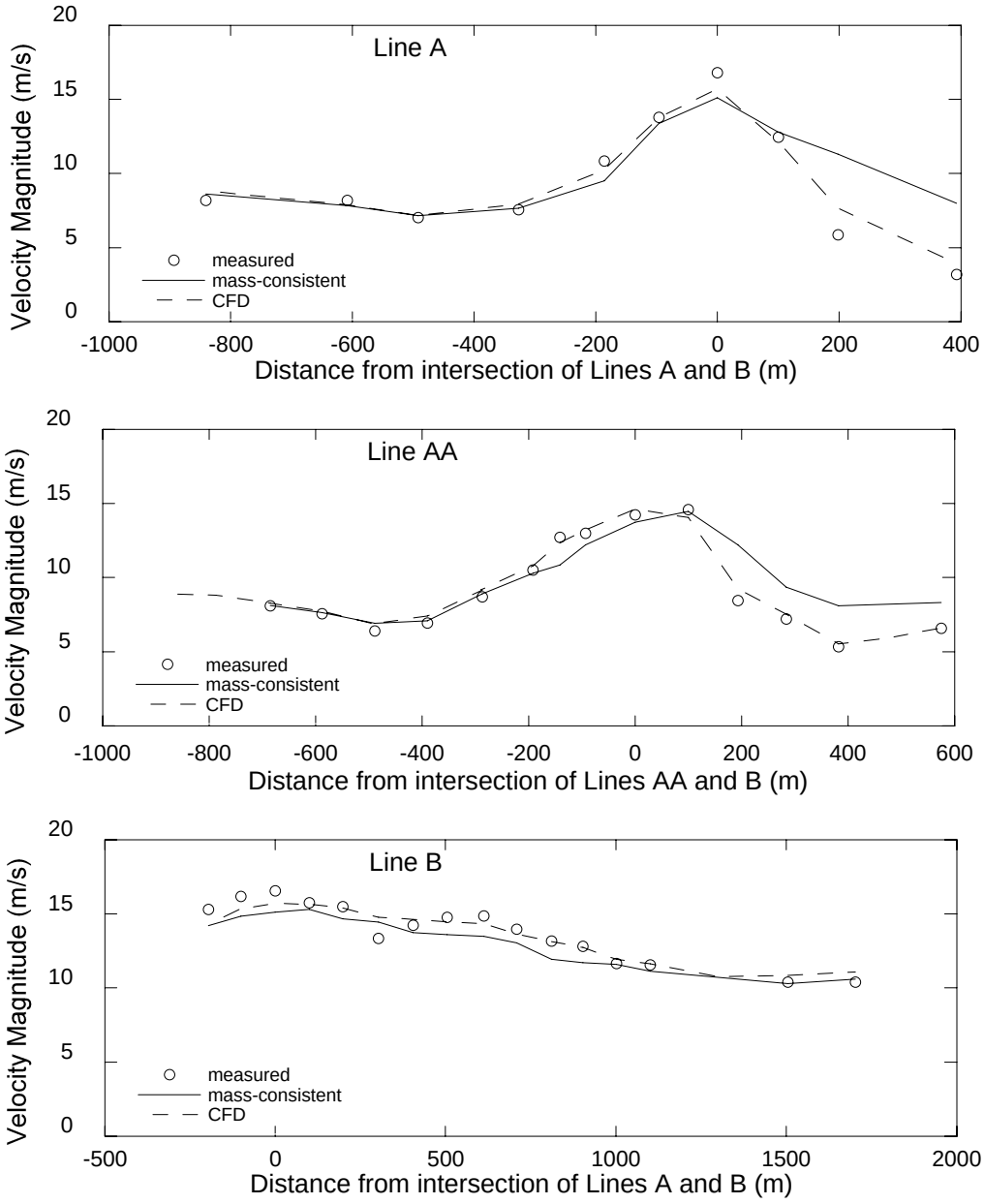

Figure 21. Simulated wind speeds from the mass-consistent and CFD models compared with measured wind speeds for Lines A, AA, and B from Figure 20 over Askervein Hill. The winds are for 10 meters above the ground.

Table 7. FARSITE inputs for the Askervein Hill simulations.

Fuel model	2
Canopy Cover	0 percent
Temperature	80 degrees F
Relative Humidity	20 percent
1 hour fuel moisture	5 percent
10 hour fuel moisture	6 percent
100 hour fuel moisture	7 percent
Live herbaceous fuel moisture	100 percent
Live woody fuel moisture	100 percent
Fire spread rate adjustments	1
Time step	10 min
Perimeter resolution	25 m
Distance resolution	25 m
Only surface fire, no spotting	

The results of the three fire simulations are shown in Figure 22. In the uniform wind case, the effect of the hill is nearly unnoticeable. The fire pattern closely resembles an ellipse. This is because the hill was not very steep and the effect of the slope on fire spread rate was far overpowered by the strong wind. The fire spread pattern for the mass-consistent wind field simulation is slightly different, but still resembles an ellipse. An increase in fire spread rate is evident near the top of the hill where the winds are strongest. Not much reduction in spread rate is seen on the lee side of the hill. The fire spread pattern for the CFD wind field is noticeably different. From ignition to just before the base of the hill the spread pattern is consistent with the other simulations. The spread rate increases slightly as the fire spreads up and over the hill top in the stronger winds, very similar to the mass-consistent simulation. Shortly past the top of the hill, a dramatic decrease in spread rate takes place. The fire has entered an area of light winds and opposing slope. This leads to a significantly lower fire spread rate on the lee side of the hill and a change in the fire shape compared to the other simulations. The slow wind speeds in the lee of the hill predicted by the CFD

wind model are verified by the wind observations, as shown in Figure 21. The mass-consistent and uniform wind fields do not have such a wind reduction. This difference in the wind fields results in a dramatic change in the resulting fire spread. It appears that, for the Askervein Hill fire simulations, the slow winds on the lee side of the hill were very important to the overall spread of the fire.

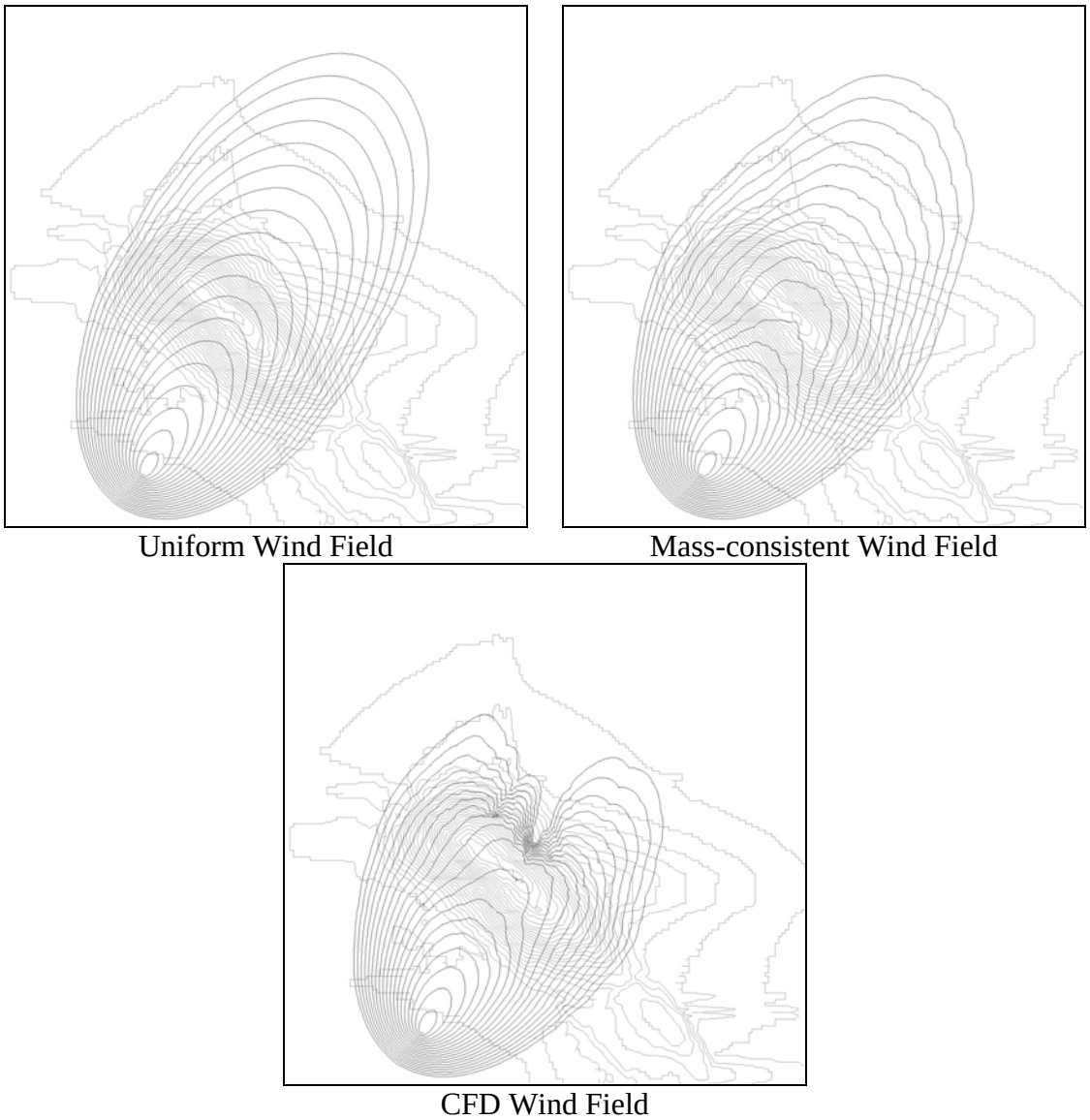

Figure 22. Comparison of three fire spread simulations for the Askervein Hill area using different wind fields. Dark lines denote the fire progression spaced 10 minutes apart, light lines are the 5 meter elevation contour lines. North is toward the top of the image.

4.4.2 South Canyon

Complex mountain winds were cited as one of the most important variables influencing the fire behavior on July 6, 1994 when the South Canyon Fire overran and killed 14 firefighters (Butler *et al.* 1998). Strong winds in excess of 50 mph developed as the result of a passing cold front. The ensuing combination of weather, fuel and terrain created extreme fire conditions that lead to the tragedy. A detailed description of the South Canyon Fire behavior is given by Butler et al. (1998). Approximate perimeters obtained from witness accounts can be found in the report. The wind conditions and abundance of published information concerning this fire make it a good candidate for study using simulations from different wind models.

Figure 23 shows an area map of the South Canyon Fire in the morning before the fire run. Twelve of the firefighters that were overrun were on the West flank fireline. The figure shows the steep, dissected terrain and the main drainage of the Colorado River to the South.

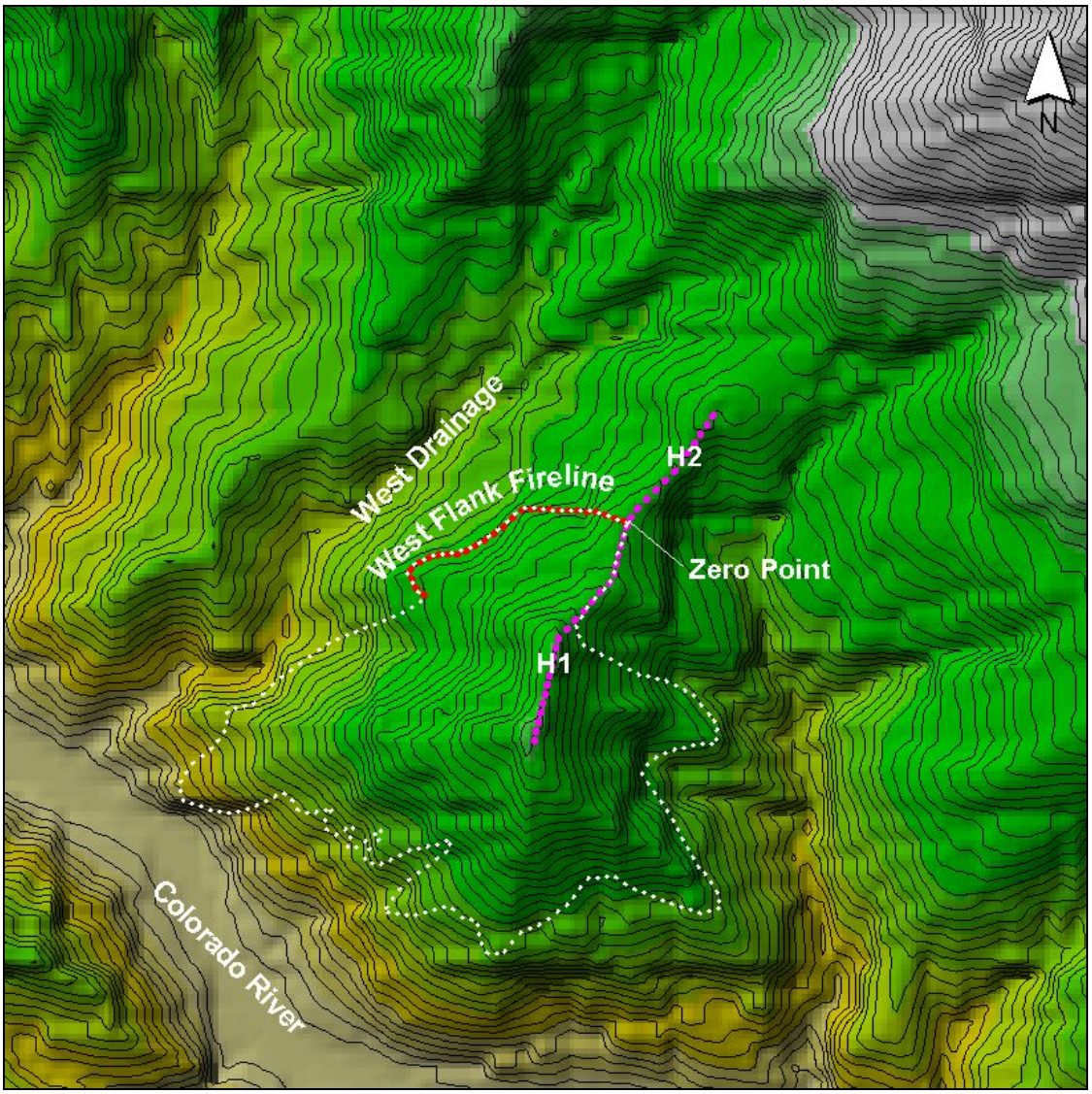

Figure 23. South Canyon Fire area map. The white dotted line indicates the fire perimeter before the blowup, the red dotted line is the West flank fireline, and the purple dotted line indicates the main ridge fireline. Helispots 1 and 2 are indicated by H1 and H2. The "Zero Point" is the point where the West flank fireline meets the ridgetop, as designated in Butler et al. (1998). The contour lines and coloring show the terrain relief.

To simulate the fire behavior using FARSITE, a fuels layer was constructed from a Digital Ortho Quad (DOQ) and descriptions of the fuels from Butler et al. (1998). The DOQ is similar to an aerial gray scale photo. The premise of classifying fuels using the DOQ is that different vegetation types reflect and emit light differently and therefore have different gray scale values in the DOQ. When this process is used on a small area and in conjunction with on the ground observations, it appears to give a

reasonable description of the fuels. The original 1 meter resolution DOQ is shown in Figure 24. The reclassification from DOQ values to standard fuel models (Anderson 1982) is shown in Table 8 and the reclassified fuels map which has been resampled to 10 meter resolution is shown in Figure 25. Most of the fuels in the fire area were modeled as fuel models 2 and 4. Canopy cover was zero percent across the landscape. Weather data from the Rifle, CO remote automated weather station (RAWS), located approximately 10 miles west of the fire location, was used for temperature and relative humidity during the simulations. The maximum temperature used for the simulations was 85 degrees F and the relative humidity was 8 percent. The RAWS recorded sustained winds up to 30 mph from the West-Southwest with gusts up to 45 mph. Butler et al. (1998) estimated the peak ridgetop winds in the fire area of over 50 mph.

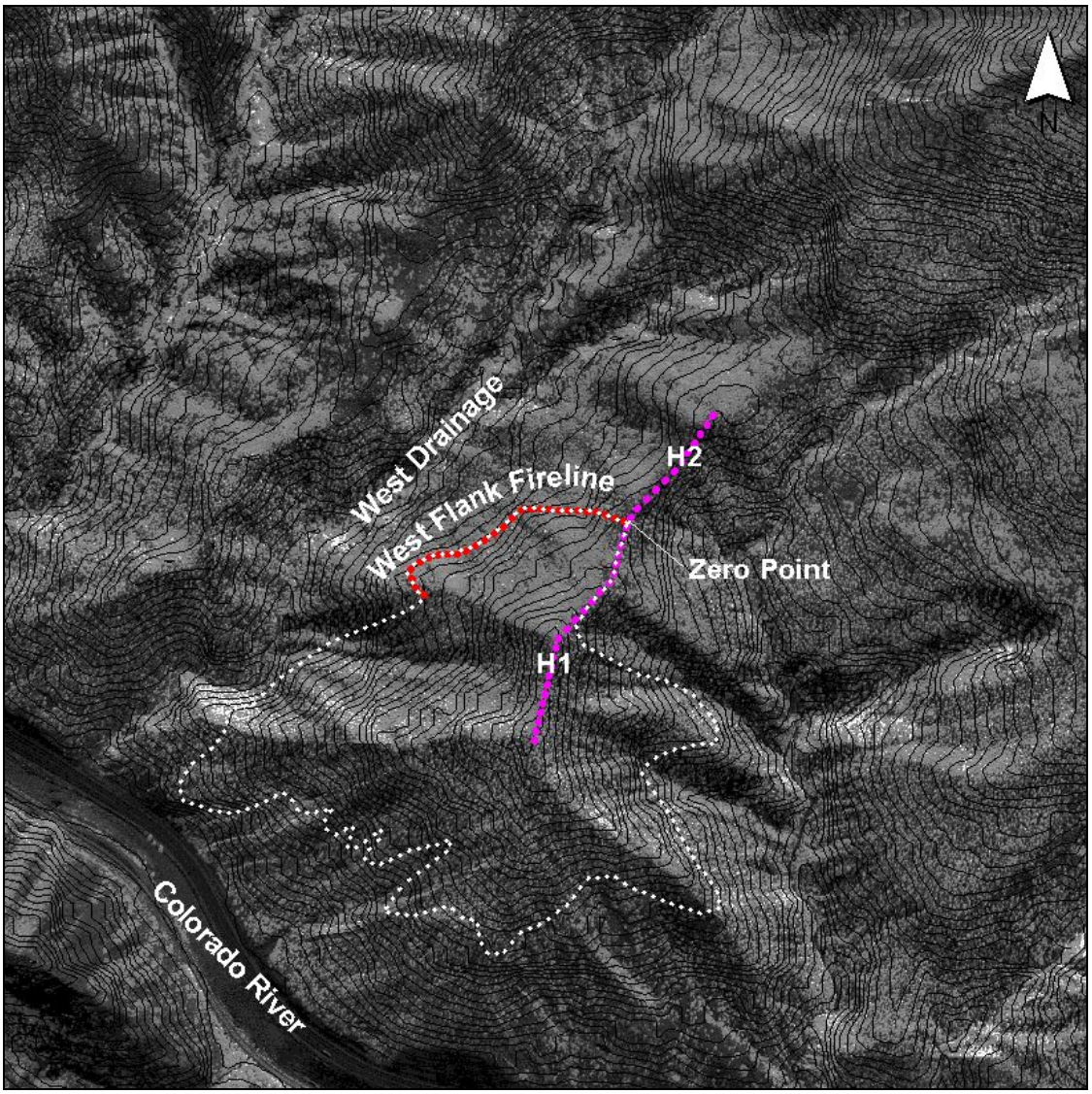

Figure 24. Original DOQ at 1 meter resolution for the South Canyon Fire. Lines and notation shown are described in Figure 23.

Table 8. South Canyon fuel model cross-walk from DOQ values.

DOQ value	Fuel model
1 – 70	10
71 – 150	4
151 – 190	2
191 – 300	99 (barren, rock)

Figure 25. Fuel model map at 10 meter resolution for the South Canyon Fire vicinity. FM 10 - dark green; FM 4 - green; FM 2 - tan; FM 99 (barren-rock) - gray. Lines and notation shown are described in Figure 23.

Wind simulations for the fire area were done on a 30 meter resolution DEM file that was 7.4 kilometers by 5.7 kilometers. Both the CFD model and the mass-consistent model were run for six different general wind directions: 180°, 225°, 240°, 250°, 260°, and 270°. These directions were chosen to bracket the observed wind directions that occurred at the time of the fire. The input speed values for each simulation were adjusted to produce 20 foot ridgetop wind speeds near Helispots 1 and

2 of 50-55 mph. For the uniform wind fields, the same six directions were used. The speed used was 33 mph. The best choice of wind speed for the uniform case is difficult to make, since it is only one speed that represents the true spatially varying wind field. No doubt, the winds near the bottom of the drainages were much lower than on the ridgetops, which is verified by witness accounts. Thirty three miles per hour was chosen here because it represents a value somewhere between the high winds reported at the ridges and the lower winds in the drainages. Also, after some preliminary fire spread simulations with the uniform winds, it was observed that this wind speed produced fire progression that best matched the observed.

Examples of the simulated winds from directions of 240 and 270 are shown in Figure 26 and Figure 27. In each figure, the top image is a mass-consistent model run and the bottom image is a CFD run. From these, it is apparent that the CFD model produces a wind field with more turning and/or channeling of the wind from terrain effects than the mass-consistent model. Both models show, in general, higher wind speeds near the ridgetops and lower wind speeds near the drainage bottoms.

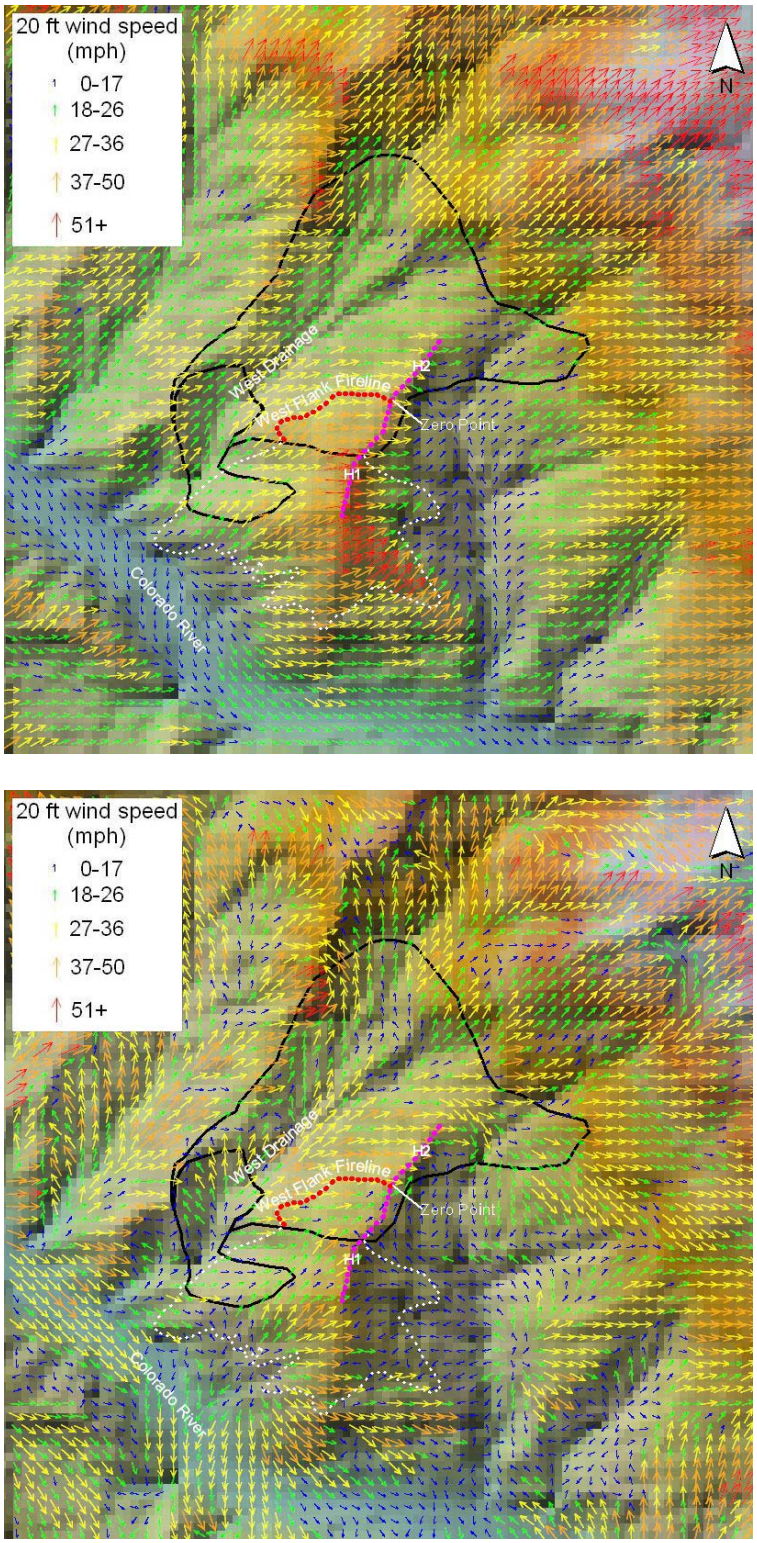

Figure 26. Wind simulations for the South Canyon Fire. The general winds are from 240 degrees. The top image is a mass-consistent model run and the bottom image is a CFD run. The two black outlines are the observed fire perimeters at 1607 and 1623.

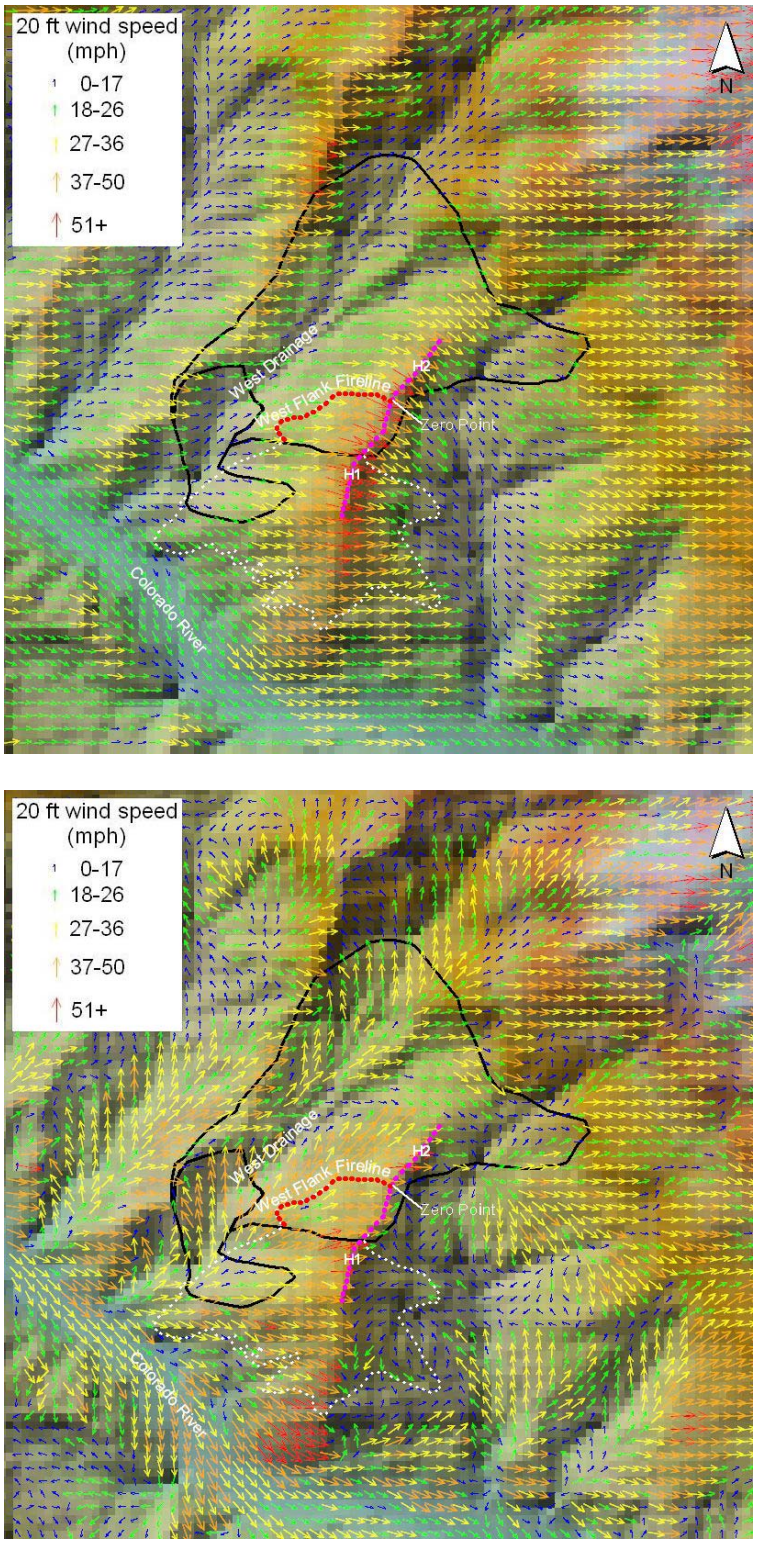

Figure 27. Wind simulations for the South Canyon Fire. The general winds are from 270 degrees. The top image is a mass-consistent model run and the bottom image is a CFD run. The two black outlines are the observed fire perimeters at 1607 and 1623.

The settings used in FARSITE for all of the fire simulations are listed in Table 9. Two parameters not included here were the "spread rate adjustment" which is a multiplier of the computed spread rate and the "percent ignition frequency" which controls how many of the lofted embers that land in burnable fuels actually start a spot fire. The spread rate adjustment factor is often used by fire analysts to quickly adjust the spread rates of a fire simulation for calibration of the model to observed fire behavior (Churchill Sanders 2001; Stratton 2006). It can partially account for problems in input such as fuel models and weather and problems in the models themselves, such as the fire spread model. The percent ignition frequency value used is difficult to justify because it is probably nearly impossible to actually know the percentage of embers that land that start spot fires. Stratton (2006) recommends starting simulations at values around 0.5-1.0% spotting ignition frequency. If spotting contributes to the growth of the real fire, then the simulation should reflect that. Butler et al. (1998) document one spot fire on the South Canyon Fire, and it is likely that many more occurred given the high wind speeds involved during the major run. For the simulations here, the percent ignition frequency of spot fires and the spread rate adjustment were adjusted to obtain the best possible agreement (visually) with the observed fire behavior for each simulation. It is acknowledged that these choices are somewhat subjective; however they have been made to match the observed perimeters as closely as possible. The goal of this modeling is to compare the effect the different wind fields have on the simulated fire progression, not to validate the spread model or fuels information. The settings for ignition frequency and spread rate adjustment are shown in Table 10.

Table 9. FARSITE settings for the South Canyon Fire simulations.

canopy cover (%)	5
stand height (m)	3
crown base height (m)	0.1
crown bulk density (kg/m^3)	0.15
canopy foliar moisture content (%)	100
canopy tree diameter (cm)	10
shade tolerance of torching trees	medium
torching species	douglas fir
initial fuel moisture - 1 hr (%)	3
initial fuel moisture - 10 hr (%)	4
initial fuel moisture - 100 hr (%)	5
initial fuel moisture - live herbacious (%)	60
initial fuel moisture - live woody (%)	60
model time step (min)	1
perimeter resolution (m)	20
distance resolution (m)	15
crown fire enabled	
crown density and cover linked	
embers from torching trees - enabled	
spot fire growth - enabled	
fire level distance checking	
fire acceleration - on	
duration: preconditioning start (day)	7/2/1994
duration: simulation start (day, time)	7/6/1994, 16:07
duration: simulation end (day, time)	7/6/1994, 16:23

Table 10. Spread rate adjustment and spot fire ignition frequencies used in the South Canyon Fire simulations.

wind model	direction (deg)	spread rate adjustment	spot fire ignition frequency (%)
CFD	270	3	3
CFD	260	2	1
CFD	250	2	1
CFD	240	1.5	1
CFD	225	3	3
CFD	180	1.5	2
mass-consistent	270	2	1
mass-consistent	260	2	1
mass-consistent	250	2	2
mass-consistent	240	2	1
mass-consistent	225	1	0.9
mass-consistent	180	1	0.9
uniform	270	1	0.8
uniform	260	1	0.8
uniform	250	1	1
uniform	240	1	1
uniform	225	1	0.8
uniform	180	1	0.8

The simulated fire spread for all of the simulations is shown in Figure 28. The FARSITE runs were started from the 16:07 polygon. A barrier was used in the simulation to prevent fire spread over the previously burned area since the fuels layer did not account for this. The final simulated and observed perimeters shown correspond to 16:23. Table 11 shows the results of the percent area comparisons. The percentages are computed using the observed burned area as the denominator, or normalizing area.

For the uniform wind images, it is apparent that the input wind direction has a large influence over the fire progression. The uniform simulations show very little fire spread in directions other than down wind. This results in a simulated fire perimeter that resembles the rough outline of an ellipse. The sensitivity of the fire spread to the

single wind direction is easily seen. Although the overall fire spread distance matches well (which is by design), the shape of the simulated perimeter does not match the observed perimeter well. In general, there is not enough lateral (cross-wind or flanking) fire spread. The percent area values for the uniform simulations shown in Table 11 also reflect the poor match. The best uniform simulation, which is wind from 240°, is coincident with the observed burned area over only 57 percent of the observed burned area.

The mass-consistent fire spread wind simulations show better agreement with the observed perimeter. For most directions, greater lateral spread of the fire is evident in the images which correlate better with the observed perimeter. In each direction, the mass-consistent runs outperformed the uniform wind runs in the percent area comparisons. The mass-consistent runs had higher coincident areas and lower under-prediction and over-prediction areas than the uniform wind runs.

From the images, it is apparent that the CFD fire spread simulations matched the observed perimeter best for most of the directions. Lateral fire spread more consistent with the observed fire behavior can be seen. In the percent area comparisons shown in Table 11, the CFD runs had higher coincident areas than the mass-consistent and uniform wind runs for all but one direction. The highest coincident area was 83.4% for the 270° run. In fact, the 240°, 250°, 260°, and 270° CFD runs all had higher coincident areas than the best mass-consistent and uniform wind runs. On average, the CFD runs had slightly more over-prediction than the mass-consistent runs but less than the uniform wind runs. If the best and worst simulations for each type of wind field are disregarded, and the remaining values are averaged, the following

coincident area averages result: 74.9% for CFD, 55.6% for mass-consistent, and 46.6% for uniform winds.

Only one direction shows obviously poor performance for the CFD runs. The 225° run largely under-predicted the fire spread, even though relatively large values of spread rate adjustment and spot fire ignition frequency were used as shown in Table 10. The wind field was to blame here, which on inspection, showed low wind speed values in the fire area. These low values occurred because of a problem with where the upwind domain boundary was located. The boundary crossed over the top of a large mountain and down to the valleys on the sides of the mountain. The specified boundary condition in the CFD wind model is that the wind speed is one uniform value along this boundary. This means that the wind speed at the top of the mountain is the same as in the valley below it. This is probably far from reality; the wind at the top is no doubt much higher than in the sheltered valley. The poor estimate on the boundary leads to a very large area of low wind speeds down wind from the mountain, which is exactly where the fire simulation took place. This did not occur for other directions because the fire area was outside of any low speed areas. This indicates that boundary placement may be important in the CFD simulations.

Figure 28. Comparison of simulated and observed fire perimeters for the South Canyon Fire. The gray shaded polygon is the 16:07 observed perimeter at the beginning of the simulations. The unfilled black lined polygon is the observed 16:23 perimeter and the filled black polygon is the simulated 1623 perimeter. The synoptic wind direction is shown on the left and the wind model used on the top.

	Uniform Wind	Mass-Consistent	CFD
180°			
225°			
240°			
250°			
260°			
270°			

Table 11. Simulated and observed percent area comparisons for the South Canyon Fire simulations.

wind model	direction (deg)	area coincident (%)	area under-predicted (%)	area over-predicted (%)
CFD	180	65.7	34.3	23.8
CFD	225	37.1	62.9	4.6
CFD	240	80.6	19.4	11.2
CFD	250	78.3	21.7	26.4
CFD	260	74.8	25.2	13.8
CFD	270	83.4	16.6	19.7
mass-consistent	180	18.5	81.5	28.7
mass-consistent	225	56.5	43.5	6.6
mass-consistent	240	73.3	26.7	10.1
mass-consistent	250	65.7	34.3	9.8
mass-consistent	260	54.1	45.9	12.9
mass-consistent	270	45.9	54.1	16.4
uniform	180	14.2	85.8	35.0
uniform	225	51.8	48.2	8.6
uniform	240	57.1	42.9	11.0
uniform	250	55.3	44.7	14.1
uniform	260	48.1	51.9	24.6
uniform	270	31.3	68.7	30.5

Overall, it appears that the behavior of the South Canyon Fire was simulated more closely using the simulated wind fields than using the spatially uniform wind. The CFD model gave the best results for all but one direction, followed by the mass-consistent model and then the uniform winds. It seems that the channeling of wind up the West Drainage was a crucial element affecting fire behavior. The CFD and mass-consistent models captured at least some of this channeling, while the uniform wind fields, of course, did not.

4.4.3 Mann Gulch

The Mann Gulch Fire overran 16 firefighters on the Helena National Forest in Montana on August 5, 1949. Only three survived. An investigation into the fire behavior on this fire was done by Rothermel (1993). The fire burned in steep terrain during a cold front passage that was characterized by winds of up to 40 mph in the open, primarily from the South. Figure 29 shows a contour plot of the fire area. Certain locations from Rothermel (1993) are shown for reference. The smokejumpers landed on the ground in Mann Gulch at 16:00 that day. They gathered their gear and hiked down Mann Gulch toward the West side of the fire. At about 17:40 they noticed that spot fires had ignited down the gulch from them and the fire was now coming up the drainage toward them. They reversed their direction and angled back up the North side of the gulch. Just before the fire overtook them, the foreman, Wag Dodge, lit an "escape fire" and lay down in the burned area for protection. The other firefighters did not understand what he was doing and continued angling uphill. The fire overtook them, only three survived, including Dodge.

Unfortunately, no documented perimeters of the fire are available. It is known, however, that the fire moved quickly up the gulch from the spot fire location, as shown in Figure 29. The fire spread from the spot fires to where the firefighters were killed in approximately 30 minutes (Rothermel 1993).

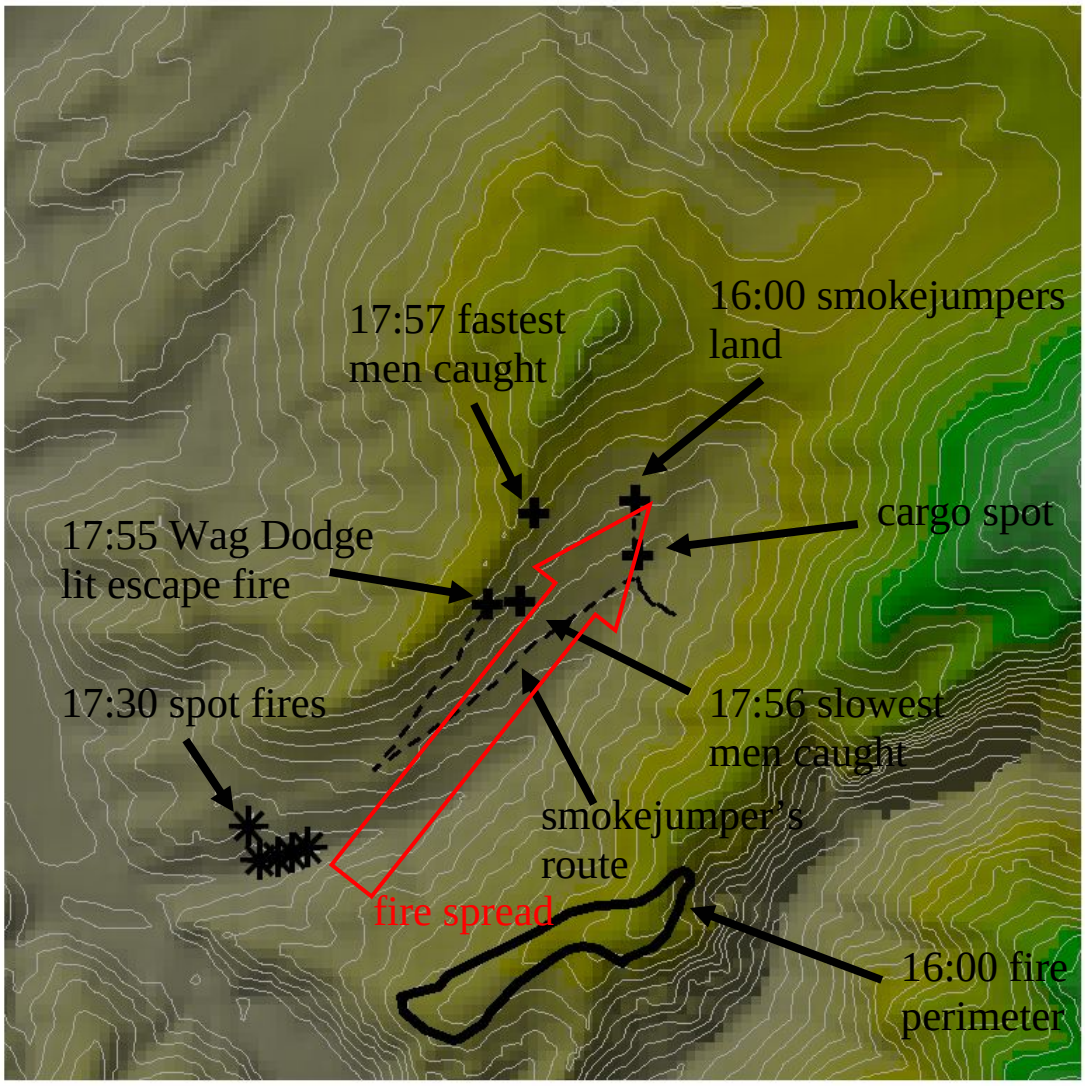

Figure 29. Elevation contour plot of the Mann Gulch Fire area. Contour spacing is 100 vertical feet. North is toward the top of the image. Locations identified are from Rothermel (1993).

The Mann Gulch Fire was simulated using FARSITE with the three different types of wind fields. Since no observed perimeters were available, the measure of how well the simulations did was determined by how well they simulated the cross-slope run up the gulch. As in the South Canyon simulations, the sensitivity of modeled fire spread to the input wind direction was examined.

Description of the fuels in the area was accomplished by adjusting LANDFIRE FBFM13 data (Rollins and Frame 2006). The adjustments were made to better reflect

the vegetation that existed during the 1949 Mann Gulch Fire, since the LANDFIRE data describes the present day (2006) condition of fuels. Visual interpretation of pre-fire aerial photos and descriptions in Rothermel (1993) were used to construct the fuels map. One adjustment made was to define all slopes of greater than 33% as rock since inspection of the aerial photos showed that the LANDFIRE data did not capture this. Fuel model 5 was changed to fuel model 2, and fuel model 8 was changed to fuel model 9 to better correspond to Rothermel's (1993) description of the fuels. On slopes with aspects between 270° and 328°, fuel model 2 was changed to fuel model 9 to correspond to the aerial photos. Also, the crown base height and canopy cover were reduced by half. These changes resulted in the fuels map shown in Figure 30. The South and East facing slope where the firefighters retreated from the fire is mainly fuel models 1 and 2. Near the top of the ridge there is a thin band of rock shown in gray.

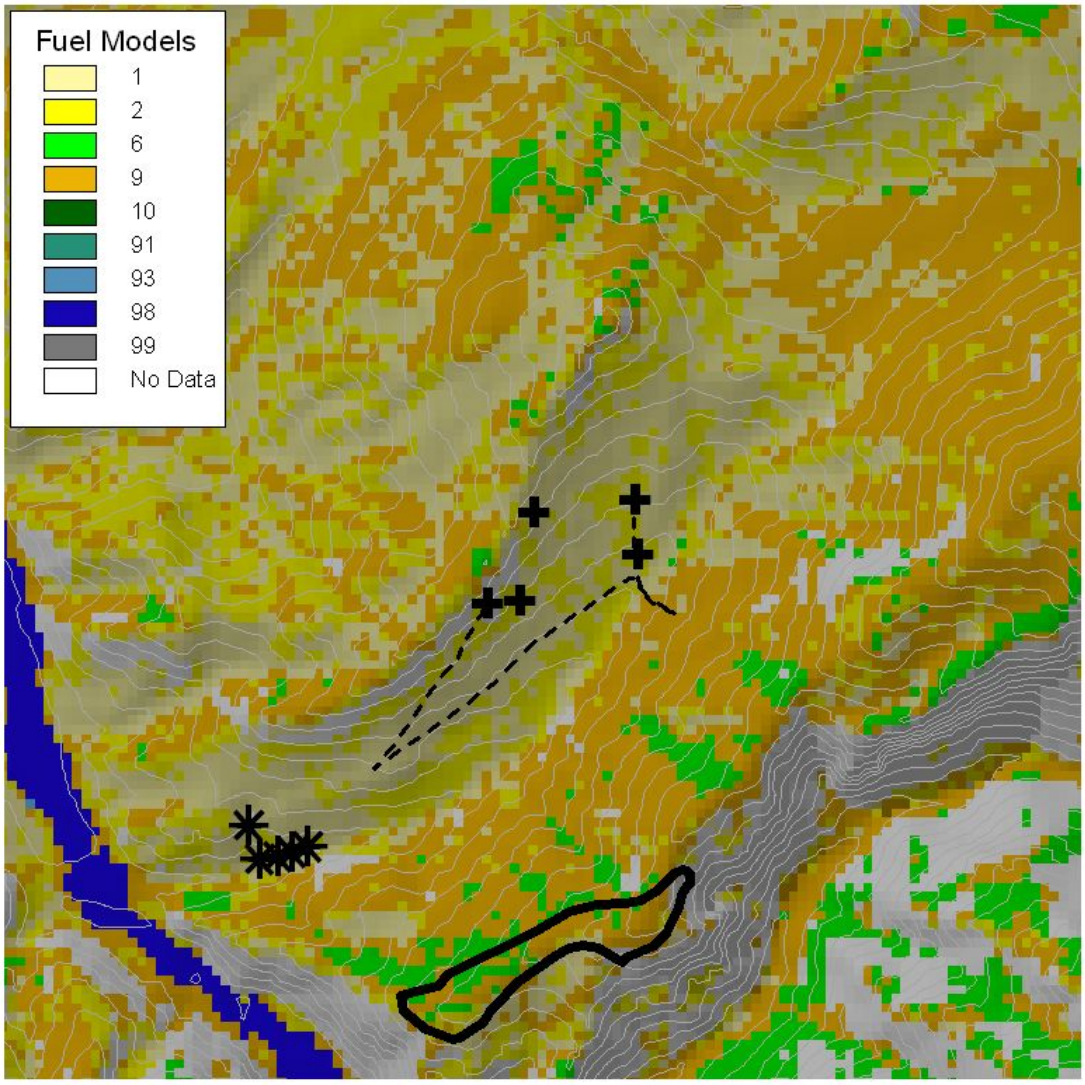

Figure 30. Fuels map used in simulations of the Mann Gulch Fire area. Contour line spacing is 100 vertical feet. North is toward the top of the image.

For the wind simulations, the modeling domain used was 22 km by 26 km. The elevation data was 30 meter resolution. Five different wind directions were used. They were 135°, 180°, 190°, 225°, and 270°. This brackets the 180° wind speed measured at the airport in Helena, MT (approximately 20 miles South-Southwest of the fire) and the 225° direction at Mann Gulch estimated by Rothermel (1993). Simulations of both the CFD wind model and the mass-consistent model were run with input speeds that gave approximately 40 mph winds near the ridgetop where the

firefighters died. The uniform wind speed used was 18 mph, which is an estimated average of the true wind field in the area. A higher speed could have been used, but it wouldn't have changed the direction the fire spread. The simulated and uniform wind fields for 180° and 270° are shown in Figure 31 and Figure 32. For both of these directions, the CFD simulations show more channeling up Mann Gulch than the mass-consistent simulations. The mass-consistent simulations do, however, show some turning of the wind up the drainage. This turning is not, of course, in the corresponding uniform wind fields. The CFD and mass-consistent wind fields also show, in general, low wind speeds near drainage bottoms and higher speeds near the tops of ridges.

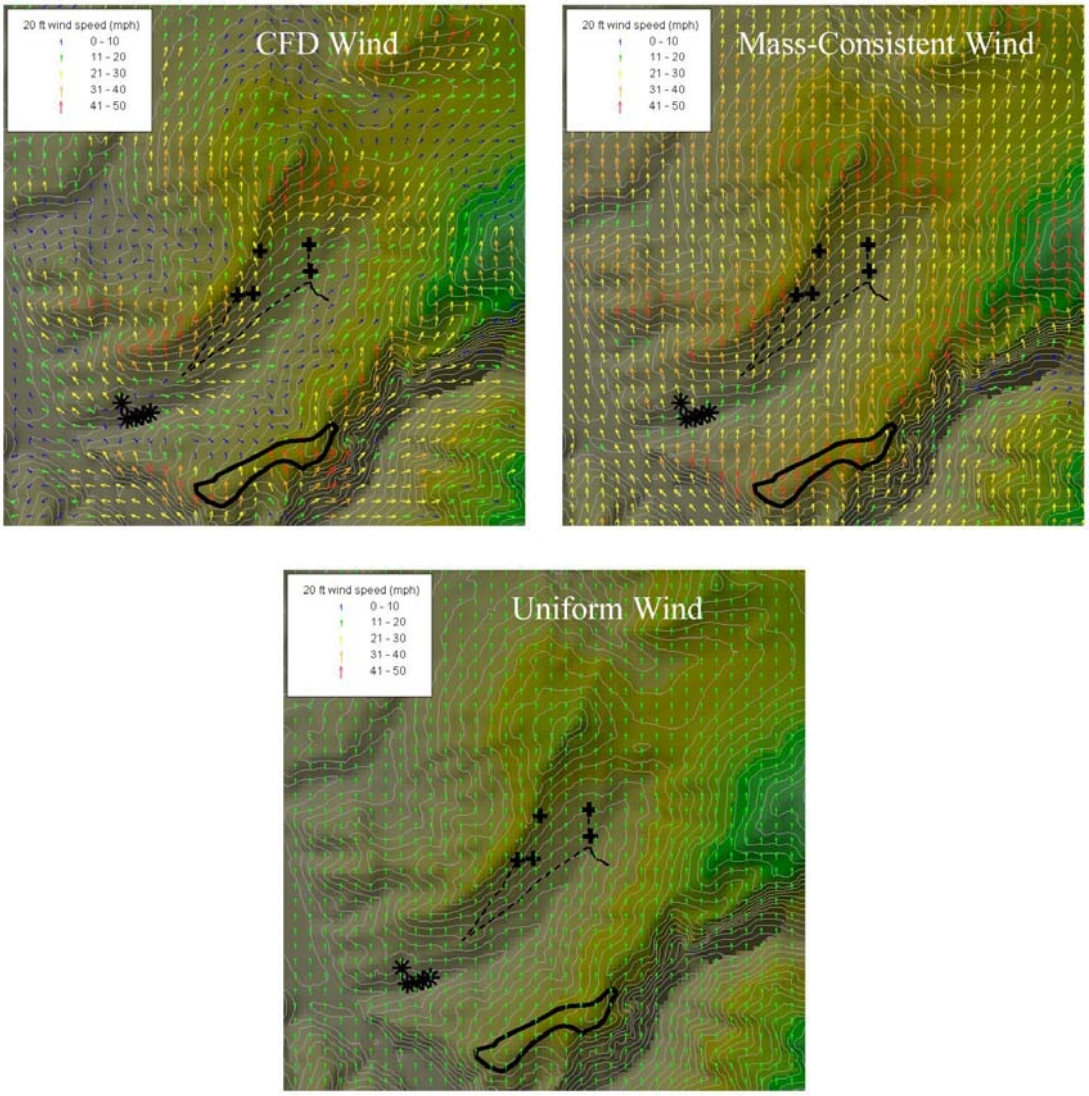

Figure 31. Wind simulations and uniform wind for the Mann Gulch Fire. Wind direction is from 180°. North is toward the top of the images.

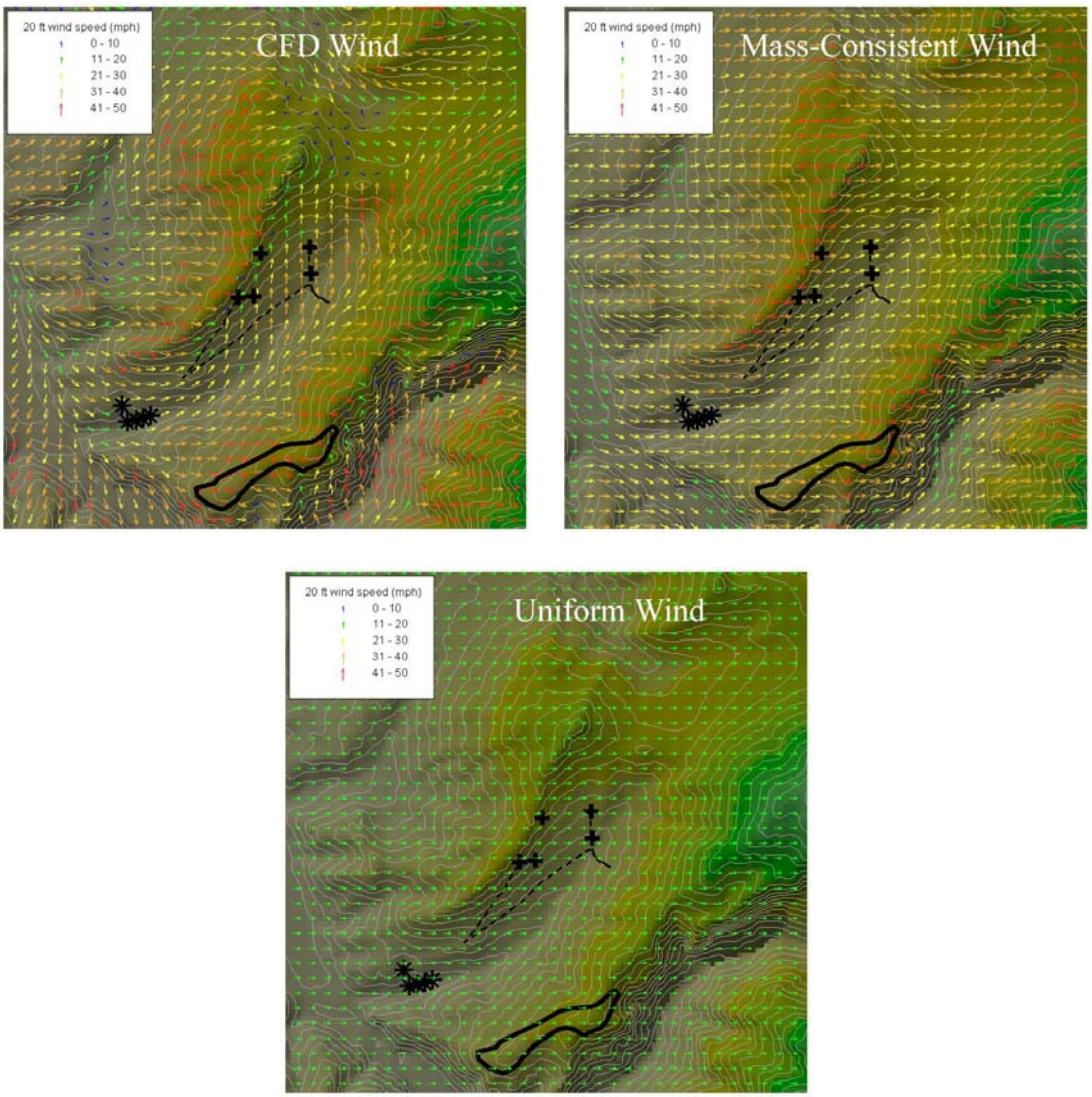

Figure 32. Wind simulations and uniform wind for the Mann Gulch Fire. Wind direction is from 270°. North is toward the top of the images.

The settings used in FARSITE are shown in Table 12. A constant spread rate adjustment of 1.8 was used for all fuels in all simulations. The simulations were started from the spot fires marked on Figure 29.

Table 12. FARSITE settings for the Mann Gulch Fire simulations.

spread rate adjustment	1.8
initial fuel moisture - 1 hr (%)	5
initial fuel moisture - 10 hr (%)	8
initial fuel moisture - 100 hr (%)	12
initial fuel moisture - live herbacious (%)	100
initial fuel moisture - live woody (%)	100
model time step (min)	3
perimeter resolution (m)	15
distance resolution (m)	15
crown fire disabled	
embers from torching trees - disabled	
spot fire growth - disabled	
fire level distance checking	
fire acceleration - on	
duration: preconditioning start (day)	8/2/1949
duration: simulation start (day, time)	8/5/1949, 1720
duration: simulation end (day, time)	8/5/1949, 1800

The simulations for the five wind directions and three different types of wind fields are shown in Figure 33. Several interesting fire patterns can be seen. The line of rock along the ridge formed a barrier to spread in many cases. In some of the simulations, the fire made it through the rock to the North of the spot fires and continued to spread.

For the 225° and 270° directions, all of the wind fields produced fire spread that moved up Mann Gulch as mainly a head fire. This matches the observed fire behavior. For the 135°, 180°, and 190° directions, none of the uniform wind field simulations result in a fire that moves far enough up Mann Gulch. The mass-consistent wind fields spread the fire slightly farther up the gulch in the 180° and 190° directions, more closely matching the observed. The mass-consistent 135° direction did not push the fire up Mann Gulch. The CFD wind fields did a much better job spreading the fire up

the gulch in the 135°, 180°, and 190° direction cases. These simulations pushed the fire past were the firefighters were killed, which is what happened in reality.

Figure 33. Fire progression from Mann Gulch simulations. The thin black lines represent the progression of the fire. The lines are spaced 3 minutes apart. The thick black line is the perimeter of the fire when the smokejumpers landed, the dashed line is the path of travel of the smokejumpers. Other markings are described in Figure 29.

	Uniform	Mass-Consistent	CFD
135°	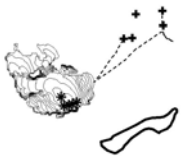	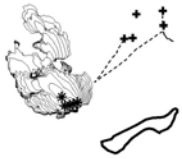	
180°			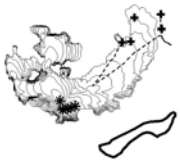
190°			
225°			
270°	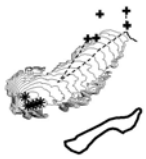		

Although the uniform, mass-consistent, and CFD fire simulations were all able to match the fire spread up Mann Gulch, the CFD fire simulations showed much less sensitivity to the input wind direction. All five directions of the CFD runs gave reasonable results, while only two of the uniform runs and about three of the mass-consistent runs matched the observed well. Although the measure of accuracy of the Mann Gulch fire simulations is subjective, the simulations do point toward the CFD wind fields producing more accurate fire simulations than the other types of wind fields. The mass-consistent runs appear to give slightly better predictions than uniform winds.

The reduced sensitivity to direction shown by the CFD fire simulations could be important to fire managers trying to predict the spread of a fire in the future. Often in these cases, weather service prediction of wind direction is not precise and covers a range of directions. The reduced sensitivity of the CFD simulations might result in more accurate fire simulations. This may be less critical in post fire analyses, if the actual wind direction is know more accurately because of onsite, witness accounts.

4.5 Conclusions

Using winds simulated with the CFD and mass-consistent models increased the accuracy of fire spread simulations for the South Canyon Fire over those based on uniform wind fields. Also, a reduction in sensitivity to input wind direction was seen in both the Mann Gulch and South Canyon Fires. This reduction in sensitivity would benefit fire modelers because the error in wind direction from weather forecasts can be high. Using uniform winds that are off by 30 degrees or more could considerably change the simulated fire spread. The winds from the mass-consistent and CFD

models appear to reduce the error that propagates through to the fire progression in complex terrain. This is probably a result of the steering and speed up/down effects present in the simulated wind fields. For example, local terrain features such as drainages tended to align the wind direction with the drainage, despite the input wind direction. The Askervein Hill case study showed that changes in wind speed can also play an important role in the spread of a fire. The low winds in the lee of the hill simulated by the CFD simulation caused a significant decrease in the spread rate of the fire when compared to the mass-consistent and uniform wind cases. It seems that the effect of local terrain features on wind flow, and as a result fire spread, can be high. This is probably most important in cases of high winds and complex terrain, however, the Askervein Hill simulations show that even simple, relatively flat terrain can cause considerable changes in wind flow and fire spread.

The CFD model performed better than the mass-consistent model and the uniform wind field. The obvious explanation is that it includes physics, eg., conservation of momentum and turbulence, that are not included in the other methods. The mass-consistent model outperformed the traditional method of using a uniform wind field. Even though the CFD model produced better fire spread simulations than the mass-consistent model, both models could probably be useful to fire managers. The advantage of the mass-consistent model is that simulations only take a few minutes compared to the CFD model which can take up to 1.5 hours. Under strict time constraints, the time savings of the mass-consistent model could justify its use over the CFD model.

CHAPTER 5. CONCLUSIONS

Two wind models have been assessed for fire management purposes. Several important conclusions have been made from this work:

1. Both the CFD and mass-consistent models describe wind flow in complex terrain better than a uniform wind field description. In most simulations, a moderate amount of error should be expected in the simulated fields due to uncertainty in inputs such as the approaching boundary layer profiles and for physics not simulated like stability effects. If the uncertainty in the inputs is high, then at the very least, the simulated winds show the relative wind behavior of different locations in the terrain.
2. The CFD model produced more accurate wind fields than the mass-consistent model. This was especially evident on the lee side of hills and ridges where momentum effects became more important. The mass-consistent model tended to over-predict wind speeds in those areas, sometimes having high errors. Also, more turning and channeling of flow was seen with the CFD model compared to the mass-consistent model.
3. The spatial variability of the simulated winds had a considerable, sometimes dramatic, effect on fire spread. Both changes in wind speed and direction caused the fire behavior to change.

4. The most accurate fire spread simulations used the CFD wind fields. The mass-consistent fire spread simulations were an improvement over the traditional uniform wind fire simulations, but showed less accuracy than the CFD simulations.
5. Fire spread was less sensitive to general input wind direction for the simulated winds compared to the traditional uniform winds. Again, the CFD was best, followed by the mass-consistent winds, and finally the uniform winds. This would benefit fire modelers attempting to model fire spread when there is uncertainty in the correct wind direction to use.
6. Although the CFD model appears to provide more accurate wind fields than the mass-consistent model, both may be appropriate for fire management because of the differences in required computing resources of each. The mass-consistent simulations generally take much less time to compute than the CFD simulations. At times it may be more practical for fire managers to use the mass-consistent model rather than the longer running CFD model.

Overall, both the CFD and mass-consistent wind models demonstrated that they would be a useful addition to fire behavior prediction systems.

Much work remains in the area of microscale wind modeling for wildland fire management use. This study has only covered a portion of the subject area. Possibilities for future work could include:

1. investigation of non-neutral atmospheric stability effects;
2. linkage with coarser meso-scale models (for initialization and/or boundary conditions);

3. spatially varying surface roughness;
4. validation in rougher, mountainous terrain;
5. evaluate the wind models in other fire spread models, possibly Prometheus (Tymstra 2007);
6. package the software so that it can be easily and successfully used by fire managers.

REFERENCES

Albini FA, Anderson EB (1982) Predicting fire behavior in U. S. Mediterrainean ecosystems. In 'Proceedings of the symposium on dynamics and management of Mediterranean-type ecosystems'. (Eds EC Conrad and WC Oechel). (USDA Forest Service General Technical Report PSW-58)

Alm LK, Nygaard TA (1995) Flow over complex terrain estimated by a general purpose Navier-Stokes solver. *Modelling, Identification and Control* **16**, 169-176.

Anderson DG, Catchpole EA, DeMestre NJ, Parkes T (1982) Modeling the spread of grass fires. *Journal of the Australian Mathematical Society* **23**, 451-466.

Anderson HE (1982) 'Aids to determining fuel models for estimating fire behavior.' USDA Forest Service, Intermountain Forest and Range Experiment Station, General Technical Report INT-122, Ogden, UT.

Andrews PL (1986) 'BEHAVE: fire behavior prediction and fuel modeling system - BURN subsystem, part 1.' USDA Forest Service, Intermountain Forest and Range Experiment Station, Gen. Tech. Rep. INT-194, Ogden, UT.

Apsley DD, Castro IP (1997) Flow and dispersion over hills: Comparison between numerical predictions and experimental data. *Journal of Wind Engineering and Industrial Aerodynamics* **67-68**, 375-386.

Arno SF, Brown JK (1991) Overcoming the paradox in managing wildland fire. *Western Wildlands* **(Spring) 40-46**.

Atkinson BW (1995) Introduction to the fluid mechanics of meso-scale flow fields. In 'Diffusion and transport of pollutants in atmospheric mesoscale flow fields'. (Ed. Dordrecht) pp. 1-20. (Kluwer Academic Publishers)

Barnard JC (1991) An evaluation of three models designed for siting wind turbines in areas of complex terrain. *Solar Energy* **46**, 283.

Barrett R, Berry M, Chan TF, Demmel J, Donato J, Dongarra J, Eijkhout V, Pozo R, Romine C (1994) 'Templates for the Solution of Linear Systems: Building Blocks for Iterative Methods, 2nd Edition.' (SIAM: Philadelphia, PA)

Boussinesq J (1877) Théorie de l'Écoulement Tourbillant. *Mem. Présentés par Divers Savants Acad. Sci. Inst. Fr.* **23**, 46-50.

Bradshaw L (2004) Wind measurements over Waterworks Hill, Missoula, MT.(U. S. Department of Agriculture, Forest Service, Rocky Mountain Research Station, Missoula Fire Science Laboratory) *unpublished work*

Butler B, Forthofer J, Finney M, McHugh C, Stratton R, Bradshaw L (2006) The impact of high resolution wind field simulations on the accuracy of fire growth predictions. In 'V International Conference on Forest Fire Research'. Figueira da Foz, Portugal. (Ed. DX Viegas)

Butler BW, Bartlette RA, Bradshaw LS, Cohen JD, Andrews PL, Putnam T, Mangan RJ (1998) 'Fire behavior associated with the 1994 South Canyon Fire on Storm King Mountain.' USDA RMRS, RP-9, Ogden, UT.

Butler BW, Forthofer JM, Finney MA, Bradshaw L (2004) High resolution wind direction and speed information for support of fire operations. In 'Monitoring Science and Technology Symposium: Unifying Knowledge for Sustainability in the Western Hemisphere'. Denver, CO. (Eds Aguirre-Bravo and Celedonio). (Procedings: U. S. Department of Agriculture, Forest Service, Rocky Mountain Research Station RMRS-P-000)

Byram GM, Nelson RM (1974) Bouyancy characteristics of a fire heat source. *Fire Technology* **10**, 68-79.

Castro FA, Palma JMLM, Silva Lopes A (2003) Simulation of the Askervein Flow. Part1: Reynolds averaged Navier-Stokes equations (k-epsilon turbulence model). *Boundary-Layer Meteorology* **107**, 501-530.

Catchpole WR, Catchpole EA, Butler BW, Rothermel RC, Morris GA, Latham DJ (1998) Rate of spread of free-burning fires in woody fuels in a wind tunnel. *Combustion Science Technology* **131**, 1-37.

Chan ST, Sugiyama G (1997) 'User's manual for MC_WIND: A new mass-consistent wind model for ARAC-3.' Lawrence Livermore National Laboratory, UCRL-MA-129067.

Chino M, Ishikawa H (1988) Experimental verification study for System for Prediction of Environmental Emergency Dose Information; SPEEDI, (I). Three-dimensional interpolation method for surface wind observations in complex terrain to produce gridded wind field. *Journal of Nuclear Science and Technology* **25**, 721-730.

Churchill Sanders KA (2001) Validation and calibration of the FARSITE fire area simulator for Yellowstone National Park. The University of Montana.

Clark TL, Jenkins MA, Coen J, Packham D (1996) A coupled atmospheric-fire model: Convective feedback on fire line dynamics. *Journa of Applied Meteorology* **35**, 875-901.

Coleman JR, Sullivan AL (1996) A real-time computer application for the prediction of fire spread across the Australian landscape. *Simulation* **67**, 230-240.

Conrad K. *The Weather Research and Forecasting Model.* Retrieved January 10, 2007 from *http://wrf-model.org/index.php*

Davis CG, Bunker SS, Mutschlecner JP (1984) Atmosperic Transport Models for Complex Terrain. *Journal of Climate and Applied Meteorology* **23**, 235-238.

Finardi S, Brusasca G, Morselli MG, Trombetti F, Tampieri F (1993) Boundary-layer flow over analytical two-dimensional hills: A systematic comparison of different models with wind tunnel data. *Boundary-Layer Meteorology* **63**, 259-291.

Finney MA (1994) Modeling the spread and behavior of prescribed natural fires. In 'Proceedings of the 12th Conference on Fire and Forest Meteorology'. Jekyll Island, GA pp. 138-143. (Society of American Foresters)

Finney MA (1995) Fire growth modeling in the Sierra Nevada of California. In 'Proceedings of the Symposium on Fire in Wilderness and Park Management'. Missoula, MT. (Eds JK Brown, RW Mutch, CW Spoon and RH Wakimoto) pp. 189-191

Finney MA (1998) 'FARSITE: Fire area simulator-model development and evaluation.' US Department of Agriculture, Forest Service, Rocky Mountain Research Station, RMRS-RP-4, Ogden, UT.

Finney MA (2000) 'Efforts at comparing simulated and observed fire growth patterns.' U. S. Department of Agriculture, Forest Service, Rocky Mountain Research Station, INT-95066-RJVA.

Fluent. *Fluent User's Guide.* Retrieved 1/28, 2007 from *www.fluent.com*

Forthofer JM, Butler BW, Shannon KS, Finney MA, Bradshaw L, Stratton RE (2003) Predicting surface winds in complex terrain for use in fire growth models. In '5th Symposium on fire and Forest Meteorology'. Orlando, FL. (American Meteorological Society)

Geai P (1987) 'Methode d'interpolation et de reconstitution tridimensionelle d'un champ de vent: le code d'analyse objective MINERVE.' EDF/DER, HE/34-87.03.

Grishin AM (1997) 'Mathematical modeling of forest fires and new methods of fighting them.' (Publishing House Tomsk University: Tomsk, Russia)

Jackson PS, Hunt JCR (1975) Turbulent wind flow over a low hill. *Quarterly Journal of the Royal Meteorological Society* **101**, 833-851.

Jones WP, Launder BE (1972) The prediction of laminarization with a two-equation model of turbulence. *International Journal of Heat and Mass Transfer* **15**, 301-314.

Kim HG, Patel VC (2000) Test of turbulence models for wind flow over terrain with separation and recirculation. *Boundary-Layer Meteorology* **94**, 5-21.

Kim HG, Patel VC, Lee CM (2000) Numerical simulation of wind flow over hilly terrain. *Journal of Wind Engineering and Industrial Aerodynamics* **87**, 45-60.

Kim S-E, Boysan F (1999) Application of CFD to environmental flows. *Journal of Wind Engineering and Industrial Aerodynamics* **81**, 145-158.

Lalas DP, Tombrou M, Petrakis M (1988) Comparison of the performance of some numerical wind energy siting codes in rough terrain. In 'European Community Wind Energy Conference'. Herning, Denmark

Lewellen WS, Sykes RI, Oliver D (1982) 'The evaluation of MATHEW/ADPIC as a real time dispersion model.' Prepared for U.S. Nuclear Regulatory Commity, NUREG/CR-2199 ARAP Rep. No. 442.

Linn RR (1997) 'Transport model for prediction of wildfire behavior.' Los Alamos National Laboratory, Scientific Report LA13334-T.

Lopes AG (2002) FireStation-an integrated software system for the numerical simulation of fire spread on complex topography. *Environmental Modeling and Software* **17**.

Lopes AMG (2003) WindStation - A software for the simulation of atmospheric flows over complex topography. *Environmental Modelling & Software* **18**, 81-96.

Mason PJ, King JC (1985) Measurements and predictions of flow and turbulence over an isolated hill of moderate slope. *Quarterly Journal of the Royal Meteorological Society* **111**, 617-640.

Maurizi A, Palma JMLM, Castro FA (1998) Numerical simulation of the atmospheric flow in a mountainous region of the North of Portugal. *Journal of Wind Engineering and Industrial Aerodynamics* **74-76**, 219-228.

Mell W, Jenkins MA, Gould J, Cheney P (2007) A physics-based approach to modeling grassland fires. *International Journal of Wildland Fire* **16**, 1-22.

Montavon C (1998) Validation of a non-hydrostatic numerical model to simulate stratified wind fields over complex topography. *Journal of Wind Engineering and Industrial Aerodynamics* **74-75**, 1762-1782.

Montero G, Montenegro R, Escobar JM (1998) A 3-D diagnostic model for wind field adjustment. *Journal of Wind Engineering and Industrial Aerodynamics* **74-76**, 249-261.

Mortensen NG, Landberg L, Troen I, Petersen EL (1993) 'Wind Atlas Analysis and Application Program (WAsP). Vol. 2: User's guide.' Riso National Laboratory, Roskilde, Denmark.

Moussiopoulos N, Flassak T (1986) Two vectorized algorithms for the effective calculations of mass-consistent flow fields. *Journal of Applied Meteorology* **25**, 847-857.

NCAR. *MM5 Community Model.* Retrieved January 10, 2007 from *http://www.mmm.ucar.edu/mm5/mm5-home.html*

NWS Internet Services Team. *The National Digital Forecast Database.* Retrieved January 10, 2007 from *http://www.weather.gov/ndfd/index.htm*

Parkinson HG (1987) Measurements of wind flow over models of a hill. University of Oxford.

Petersen EL, Mortensen NG, Landberg L, Hojstrup J, Frank HP (1997) 'Wind Power Meteorology.' Riso National Laboratory, Wind Energy Department, Riso-I-1206(EN), Roskilde, Denmark.

Porterie B, Morvan D, Loraud JC, Larini M (2000) Fire spread through fuel beds: Modeling of wind-aided fires and induced hydrodynamics. *Physics of Fluids* **12**, 1762-1782.

Raithby GD, Stubley GD (1987) The Askervein Hill Project: A finite control volume prediction of three-dimensional flows over the hill. *Boundary-Layer Meteorology* **39**, 247-267.

Ratto CF, Festa R, Nicora O, Mosiello R, Ricci A, Lalas DP, Frumento OA (1990) Wind field numerical simulations: a new user-friendly code. In '1990 European Community Wind Energy Conference'. Madrid, Spain. (Ed. W Palz). (H. S. Stephens & Associates)

Ratto CF, Festa R, Romeo C, Frumento OA, Galluzzi M (1994) Mass-consistent models for wind fields over complex terrain: The state of the art. *Environmental Software* **9**, 247-268.

Richards P, Hoxey R (1993) Appropriate boundary conditions for computational wind engineering models using the k-epsilon turbulence model. *Journal of Wind Engineering and Industrial Aerodynamics* **46-47**, 145-153.

Rollins MG, Frame CK (2006) 'The LANDFIRE Prototype Project: nationally consistent and locally relevant geospatial data for wildland fire management.' U. S. Department of Agriculture, Forest Service, Rocky Mountain Research Station, General Technical Report RMRS-GTR-175, Fort Collins, CO.

Ross DG, Smith IN, Manins PC, Fox DG (1988) Diagnostic Wind Field Modeling for Complex Terrain: Model Development and Testing. *Journal of Applied Meteorology* **27**, 785-796.

Rothermel RC (1972) 'A mathematical model for predicting fire spread in wildland fuels.' USDA Forest Service Research Paper INT-115, Ogden, UT.

Rothermel RC (1993) 'Mann Gulch Fire: A race that couldn't be won.' USDA Forest Service, Intermountain Research Station, INT-299, Ogden, UT.

Rykiel EJ (1996) Testing ecological models: the meaning of validation. *Ecological Modeling* **90**, 229-244.

Sanderlin JC, Van Gelder RJ (1977) A simulation of fire behavior and suppression effectiveness for operation support in wildland fire management. In 'Proceedings of the 1st International Convention on mathematical modeling'. St. Louis, MO pp. 619-630

Sasaki Y (1958) An objective analysis based on the variational method. *Journal of the meteorological society of Japan* **36**, 77-88.

Sasaki Y (1970a) Numerical variational analysis formulated under the constraints determined by longwave equations and low-pass filter. *Monthly Weather Review* **98**, 884-898.

Sasaki Y (1970b) Some basic formalisms in numerical variational analysis. *Monthly Weather Review* **98**, 875-883.

Scire JS, Robe FR, Fernau ME, Yamartino RJ (2000) 'A user's guide for the CALMET meteorological model.' Earth Tech, Inc., Concord, MA.

Sherman CA (1978) A mass-consistent model for wind fields over complex terrain. *Journal of Applied Meteorology* **17**, 312-319.

Stangroom P (2004) CFD modeling of wind flow over terrain. The University of Nottingham.

Stratton RD (2006) 'Guidance on spatial wildland fire analysis: models, tools, and techniques.' U. S. Department of Agriculture, Forest Service, Rocky Mountain Research Station, General Technical Report RMRS-GTR-183, Fort Collins, CO.

Taylor PA, Teunissen HW (1983) 'Askervein '82: Report on the September/October 1982 Experiment to study boundary layer flow over Askervein, South Uist.' Atmospheric Environment Service, MSRB-83-8, Downsview, Ontario.

Taylor PA, Teunissen HW (1985) 'The Askervein Hill Project: Report on the September/October 1983 Main Field Experiment.' Atmospheric Environment Service, MSRB-84-6, Downsview, Ontario.

Thompson EG (2005) 'Introduction to the Finite Element Method: Theory, Programming, and Applications.' (John Wiley & Sons, Inc.: USA)

Tombrou M, Lalas DP (1990) A telescoping procedure for local wind energy potential assessment. In 'Resource assessment. European Community Wind Energy Conference'. Madrid. (Ed. W Palz). (H. S. Stephens & Associates)

Tymstra C. *Prometheus: The Canadian wildland fire growth model.* Retrieved 3/8, 2007 from *www.firegrowthmodel.com*

Uchida T, Ohya Y (1999) Numerical simulation of atmospheric flow over complex terrain. *Journal of Wind Engineering and Industrial Aerodynamics* **81**, 283-293.

Undheim O, Andersson HI, Berge E (2006) Non-linear, microscale modelling of th flow over Askervein Hill. *Boundary-Layer Meteorology*.

USDA Forest Service and USDI Bureau of Land Management (2002) 'Price Canyon Fire Entrapment Investigation Report.' Missoula, MT.

USGS. *Fire data ordering system.* Retrieved 8/25, 2006 from *http://firedata.cr.usgs.gov*

Van Wagner CE (1977) Conditions for the start and spread of crown fire. *Canadian Journal of Forest Research* **7**, 23-34.

Vandoormaal JP, Raithby GD (1984) Enhancements of the SIMPLE method for predicting incompressible fluid flows. *Numerical Heat Transfer* **7**, 147-163.

Walmsley JL, Taylor PA (1996) Boundary-layer flow over topography: Impacts of the Askervein Study. *Boundary-Layer Meteorology* **78**, 291-320.

Walmsley JL, Taylor PA, Keith T (1986) A simple model of neutrally stratified boundary layer flow over complex terrain with surface roughness modulations (MS3DJH/3R). *Boundary-Layer Meteorology* **36**, 157-186.

Walmsley JL, Troen IB, Demetrius P, Lalas DP, Mason PJ (1990) Surface-layer flow in complex terrain: Comparison of models and full-scale observations. *Boundary-Layer Meteorology* **52**, 259-281.

Wierenga J (1993) Representative roughness parameters for homogenous terrain. *Boundary Layer Meteorology* **63**, 323-363.

Xu J, Lathrop RG (1994) Geographic information system based wildfire spread simulation. In '12th Conference on Fire and Forest Meteorology' pp. 477-484

Yakhot V, Orszag SA (1986) Renormalization group analysis of turbulence. I. Basic theory. *Journal of Scientific Computations* **1**, 3-51.